TITOLO **Comparison of integrated and decoupled Monte Carlo results outside PWR cores**

AUTORI P. Console Camprini, K. W. Burn [1], and M. Brovchenko [2]

[1] former ENEA researcher

[2] IRSN (Institut de Radioprotection et de Sûreté Nucléaire)

SOMMARIO This article considers two ex-core PWR sample problems and compares the single eigenvalue approach with an all Monte-Carlo decoupled approach with different approximations at the point of decoupling. It provides support and technical background to a journal article that contains the principal results. This pair of articles constitutes the second part, focusing on comparison with PWR GEN II and GEN III ex-core decoupled results, of an extended paper – the first part concentrated on methodology.

REDAZIONE	CONTROLLATO	APPROVATO
P. Console Camprini	M. Tarantino	M. Tarantino
	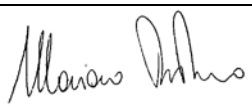	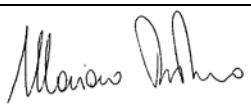

Revision	Date	Scope of revision	Page
0	20/12/2021	Prima stesura/First Issue	39
1	02/09/2022	Improved description of Fig.4, removal of 1st paragraph of §3.2.4, modification of figure numbers cited in [1] and of the last paragraph of page 31: substitute §4.1 for §3.2.2.2	39

TABLE OF CONTENTS

1. INTRODUCTION

This paper provides support and background to an article [1] that contains the principal results and discussion. Such article is the second part of a paper that assesses an approach that has been developed to calculate differential in- and ex-fissile configuration responses employing Monte Carlo with variance reduction (VR).

The first part [2] focused more on the methodological aspects and considered how a single eigenvalue calculation could be made as efficient as possible, as compared with an empirical methodology (involving again a single eigenvalue calculation). Instead, the second part [1] compares the approach to various decoupling approximations. The comparison is made through the evaluation of a number of ex-core responses of two PWR models, GEN II and GEN III. (It may be mentioned that in [2] an in-core problem is also treated.)

The ex-core problems involve the radiation damage to the pressure vessel (PV) and the ex-core neutron detector signal in the PV well of the two PWR models. In the PWR GEN III model (which is the same geometric model as in part I [2] but with a slightly different core composition), we also consider activation responses in the concrete shielding surrounding the PV well.

2. PWR GEN II

The PWR GEN II model has a standard arrangement of baffle – water reflector – barrel with neutron pads in the inner part of the downcomer. A vertical section is shown in Fig. 1. The PV damage was evaluated on the inner surface of the PV at the core mid-plane at a number of azimuthal positions shown in Fig. 2. Each position subtended an azimuthal angle of 2° and extended over a height of 20 cm. Fig. 2 also shows the positions of the two ex-core detectors.

A vertical section through the ex-core detectors is shown in Fig. 3. Fig. 4 shows a horizontal section of the ex-core detector at 45°. A thin amorphous film of ^{10}B, not modelled in the transport, was assumed to cover the inner surface over the central ½ height of the detector.

The responses of interest were the total neutron fluxes with energy above 1 MeV and above 100 keV at the various positions on the PV and the $^{10}B(n,\alpha)$ reaction rate in the film of the ex-core detectors. An average of the responses from both detectors was taken.

End-of-cycle MOX assembly-wise fuel compositions were employed with no axial variation. The ^{235}U / ^{239}Pu ratio had a range varying from less than 0.1 to around 10, depending on the assembly.

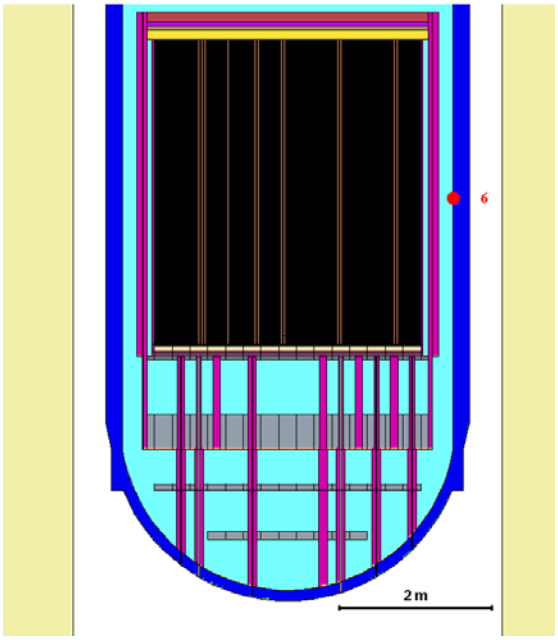

Figure 1. PWR GEN II: Vertical section

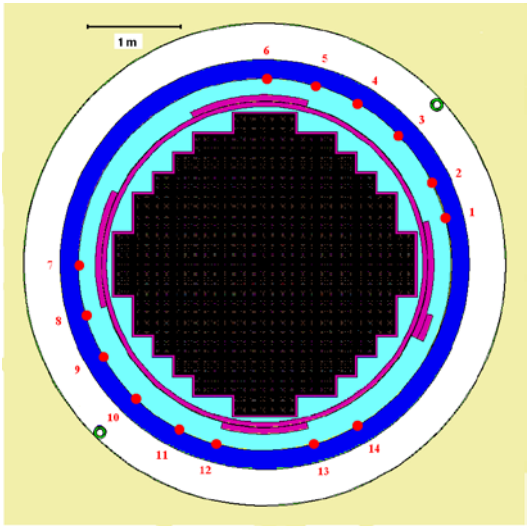

Figure 2. PWR GEN II: Horizontal section at the core mid-plane

2.1 METHODOLOGY

The single eigenvalue calculation employed by the new approach used a superhistory [3] of 10 fission generations without fictitious source cells (defined in [2]). Fission energy deposition tallies (type 7 [4]) in each of 12 fission zone segments (3 radial and 4 symmetric segments) were employed to model the global responses [2]. These 12 fissile zone segments were identical to those that were subsequently employed for the VR. Further details of the methodology may be found in [2].

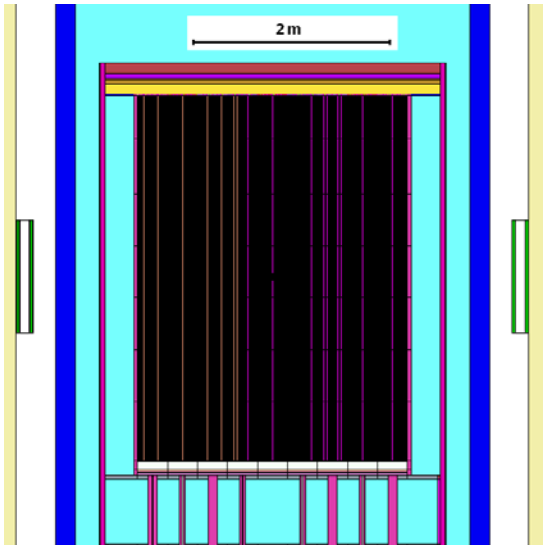

Figure 3. PWR GEN II: Vertical section with ex-core detectors

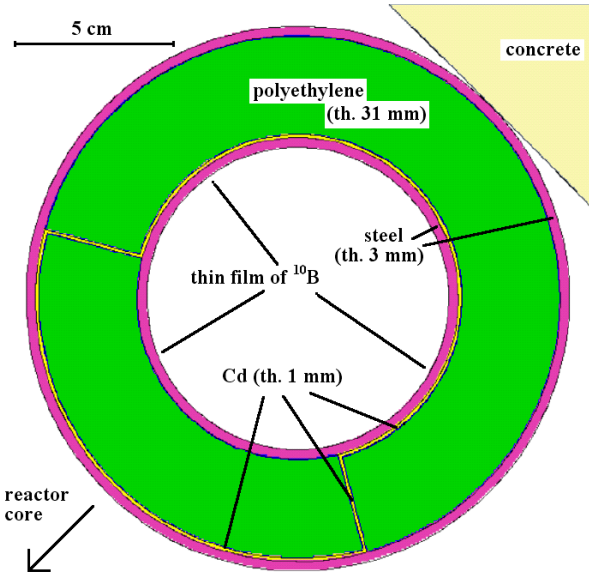

Figure 4. PWR GEN II: ex-core detector horizontal section

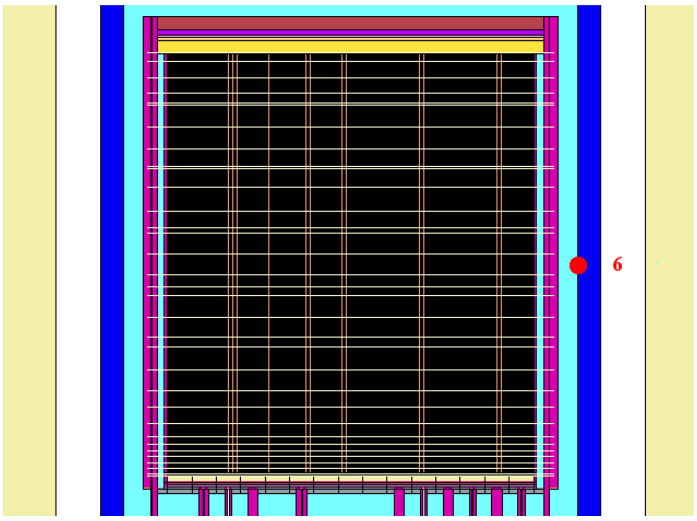

Figure 5. PWR GEN II: Axial division of fissile zone for decoupling

The point of decoupling in the decoupled calculations was the fission sites. The axial binning of the fission sites was with 32 bins in the structure shown in Fig. 5. Radial binning was pin-wise with each pin divided into two radial segments of equal area. Each radial segment had its own axial distribution. We called this the “dual pin-wise description” of the fission sites. An assembly-wise radial binning was also modelled for the ex-core neutron detector. In this case each assembly had its own axial distribution. We called this the “assembly-wise description” of the fission sites.

The first part of the decoupled calculation that wrote the fission source was an eigenvalue calculation with no VR (and without superhistories). After reaching the fundamental mode, 10^6 neutrons per fission generation and 500 fission generations were run. The fission sites in the appropriate spatial binning were written to a *MCTAL* file [4]. The statistical error in this calculation, although small, did not appear in the final error estimates.

In the second part of the decoupled calculation the neutron energy was selected from three different Watt fission spectra with parameters corresponding to the MCNP default [4], fission of ^{235}U and of ^{239}Pu, the latter two induced by thermal neutrons [4]. Note that MCNP required modification of the *source* subroutine to accept the pin-wise source.

The VR for the second part of the decoupled calculation was taken from the eigenvalue case with parameters generated by the DSA then converted to a weight window [4].

Finally three calculations were made with each of the three energy spectra and a homogeneous spatial distribution of the fission sites throughout the core (including cladding and coolant, delimited by the outer surfaces of the assemblies).

2.2 RESULTS

All the results were normalized to 1 watt of thermal power (assuming that this included 7.07% decay heat, we calculated a corresponding neutron source of 8.16×10^{10} neutrons / sec[1]). Two standard deviation error bars are present in all the figures but may be concealed by the data points.

Fig. 6 shows the neutron fluxes at the various positions at the inner surface of the PV from the eigenvalue calculation. Statistical errors were calculated between superhistories (10 fission generations). The ex-core neutron detector signal was 320.85 ^{10}B(n,α) reactions per sec with a (single) standard deviation of ±1.16.

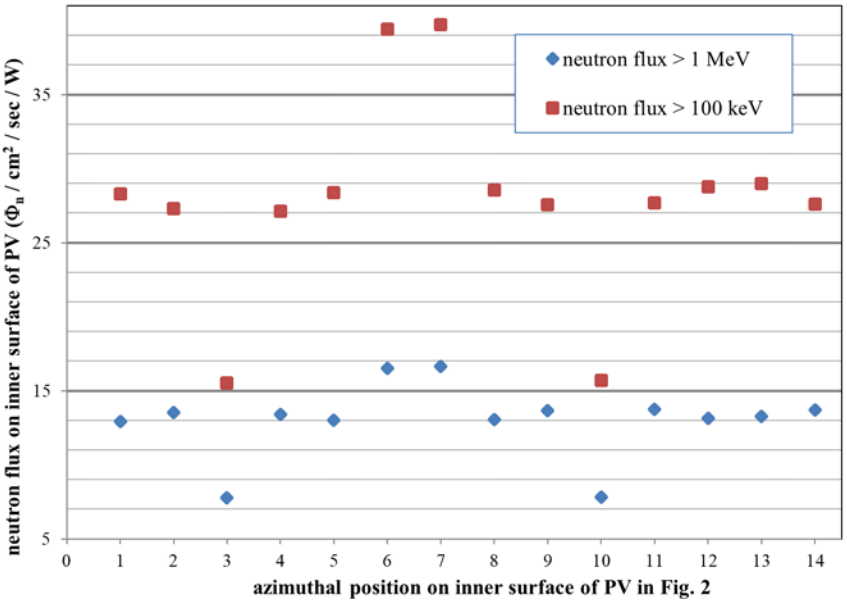

Figure 6. PWR GEN II: Neutron fluxes on the inner surface of the PV at the core mid-plane

The ratio: decoupled result to eigenvalue result, with the dual pin-wise description (plus assembly-wise description for the ex-core detectors) and with the source spectra: default, ^{235}U and ^{239}Pu in

[1] With MCNP we employed a +F6 tally [4] over all in- and ex-core cells in a coupled neutron-photon calculation and obtained 71.08 MeV per source fission neutron. This (prompt) energy deposition value was actually just under 5% greater than the result of a F7:n tally over all in-core cells.

the second part of the decoupled calculation, is shown in Figs. 6 – 8 respectively in [1].

Figs. 7 – 9 show the same ratio: decoupled result to eigenvalue result, for the three source spectra: default, ^{235}U and ^{239}Pu respectively, for the homogeneous spatial distribution of the fission sites. The errors in these figures take into account both the statistical error in the eigenvalue calculation and that in the second part of the decoupled calculation, but not the statistical error in the first part of the decoupled calculation.

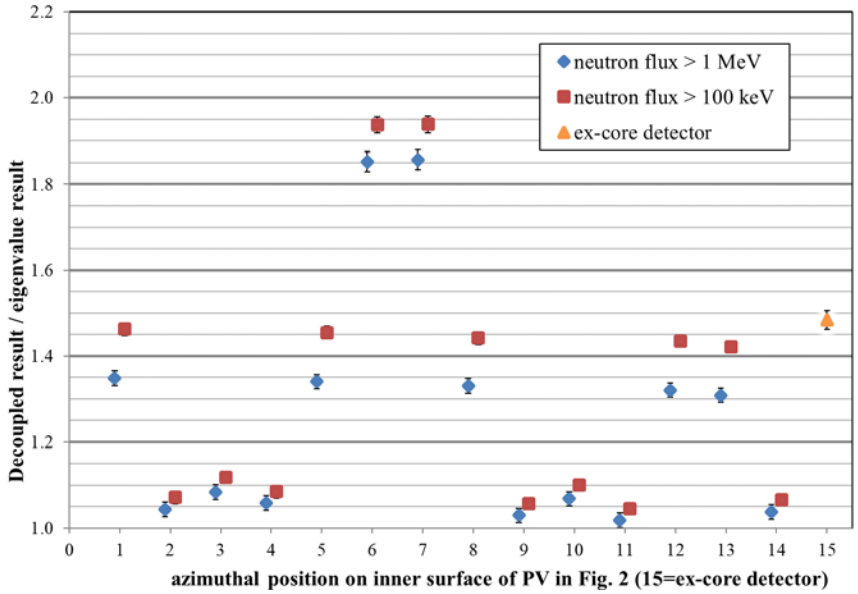

Figure 7. PWR GEN II: Ratio of decoupled to eigenvalue result for the MCNP default Watt fission spectrum and a homogeneous spatial distribution of fission sites

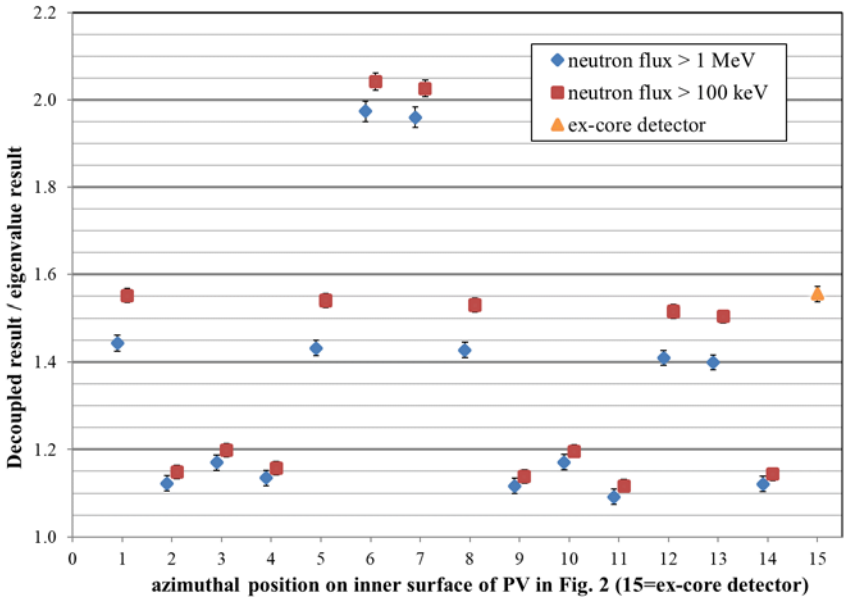

Figure 8. PWR GEN II: Ratio of decoupled to eigenvalue result for the Watt spectrum for thermal neutron-induced fission on 235U and a homogeneous spatial distribution of fission sites

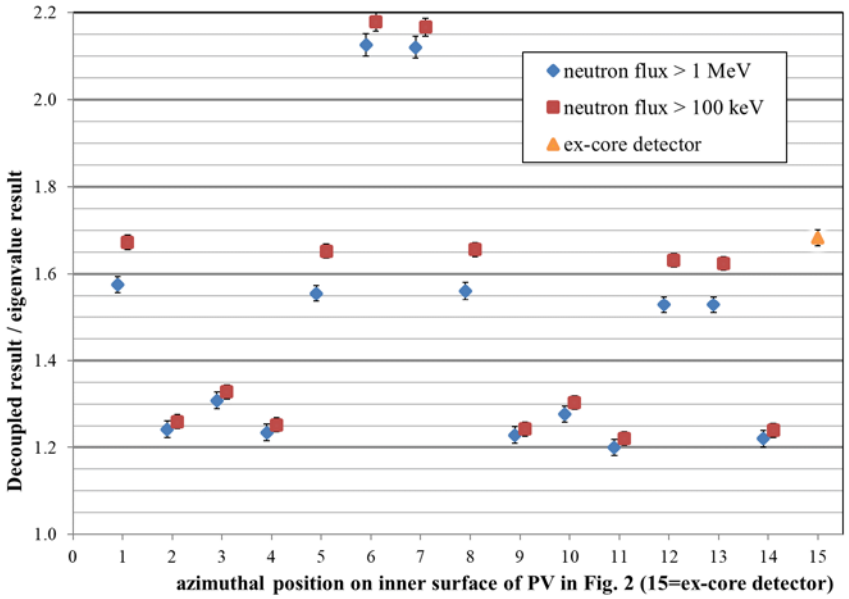

Figure 9. PWR GEN II: Ratio of decoupled to eigenvalue result for the Watt spectrum for thermal neutron-induced fission on 239Pu and a homogeneous spatial distribution of fission sites

From Figs. 7 – 9 we see that for the homogeneous source:

- The results at the 14 positions on the PV are much more scattered than those in Figs. 6 – 8 in [1] for the dual pin-wise approximation. However, there is the same tendency for each of the three spectra: positions 2-4, 9-11 and 14 have ratios that are lower, positions 6 and 7 are higher and positions 1, 5, 8, 12 and 13 are in the middle band.
- The ex-core detector ratios are situated in the middle band.
- The results are in the range 1 – 2.2 (compare 0.85 – 1.1 for the dual pin-wise results in [1]).
- The 100 keV ratios in the middle and upper bands are higher than the 1 MeV ratios. The difference is greater for the positions 1, 5, 8, 12-13 that are in the middle band.
- The results increase going from the default, to the ^{235}U, to the ^{239}Pu spectrum, as for the dual pin-wise results in [1].

3. PWR GEN III WITH THICK STEEL REFLECTOR

Notwithstanding the fact that the MCNP model used in this study contains a very approximate description in terms of geometry and composition of internals and elements outside the vessel, it is considered as representative for radiation attenuation purposes.

End-of-cycle MOX assembly-wise fuel compositions were employed with no axial variation. The ^{235}U / ^{239}Pu ratio ranged from around 0.5 to 5 depending on the assembly.

An important difference from the GEN-II model of §2 is the presence of a radial steel reflector just outside the core. This is visible in Figs. 10 – 12. Fig. 10 shows a vertical section of the GEN-III reactor model. Figs. 11 and 12 show horizontal sections at the core mid-plane. Figs. 13 and 14 show horizontal sections at and just below the platforms respectively.

There were three sets of responses. The first set measured damage at the internal surface of the PV and included both neutron and γ responses. The second set was an ex-core neutron detector in the PV well similar to the one in the previous PWR GEN II example. The third set consisted of a number of activation rates of isotopes commonly found in concrete and rebar in the concrete shielding surrounding the PV well. We also included in this set the neutron dose [5].

The two principal gauges of the vessel damage are the neutron fluxes with energy above 1 MeV and above 100 keV. Here we also employed dpa (displacements per atom), both neutron-induced [6] and γ-induced (for Fe only, Table 3 in [7] – note that the threshold for γ-induced dpa is 700 keV). The three heights where the PV damage is evaluated are shown in Fig. 10 as red dots (at the core mid-plane, at the supporting platforms and just below the platforms at the nearest point of the lower, thinner part of the PV to the core).

There are four azimuthal positions at the core mid-plane and just below the platforms: A1 – A4 in Fig. 11 and C1 – C4 in Fig. 14, and two positions at the platforms: B1, B2 in Fig. 13. Thus there are 4 requested results at each of 10 positions making 40 responses. Each position at the mid-plane and below the platform subtends an azimuthal angle of 2° and has a height of 20 cm. The two positions at the platform are slightly larger.

The ex-core neutron detector was similar to the one employed in the PWR GEN II model (Fig. 4). Its location is shown in Figs. 15 and 16. We took the average signal from the 4 detectors. As for PWR GEN II we assumed that the sensitive part of the detector occupied the central axial part over ½ the physical length.

At depths of 15 cm and 150 cm in the radial concrete shielding (Fig. 17), the following activation rates were considered: $^{59}Co(n,\gamma)$, $^{151}Eu(n,\gamma)$, $^{153}Eu(n,\gamma)$, $^{54}Fe(n,\gamma)$ and $^{56}Fe(n,2n)$. Note that the (n,2n) reaction has a threshold at around 11.5 MeV. The Fe was in rebar (assumed 3% by vol. mixed homogeneously in the concrete). The Co was assumed 100 ppm by weight in the rebar. The Eu was assumed 4 ppm by weight in the concrete. We tallied these responses over a height equal to that of the fissile zone and on 360°.

3.1 METHODOLOGY

The methodology is similar to that of the GEN II model in §2.1. The single eigenvalue calculation of the new approach employed a superhistory [3] of 10 fission generations without fictitious source cells [2]. Again to model the global responses, fission energy deposition tallies (type 7 [4]) were employed, the fissile zone was divided into 12 segments (3 radial and 4 axial) and the 40 ex-core responses were mocked up by 24 local responses (just to generate the VR parameters). The 12 fissile zone segments were identical to those that were subsequently employed for the VR. Further discussion of the methodology may be found in [2].

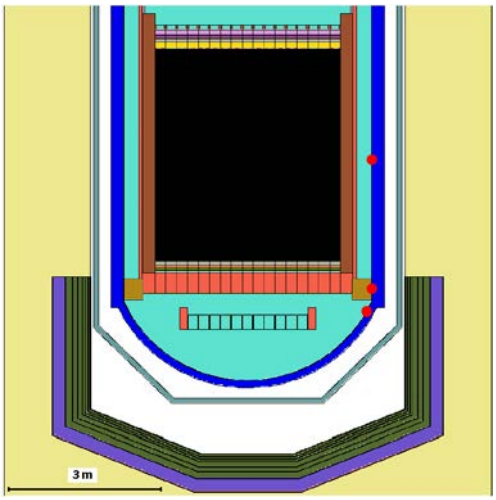

Figure 10. PWR GEN III: Vertical section

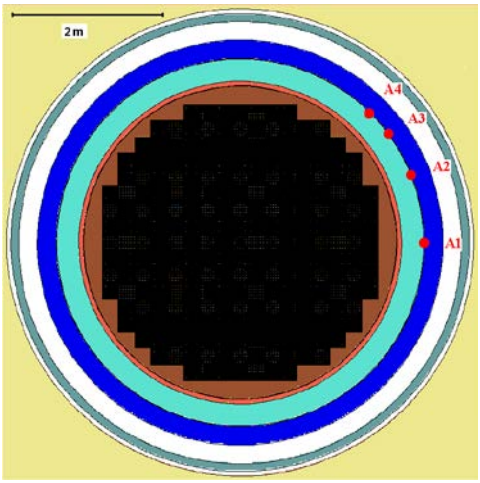

Figure 11. PWR GEN III: Horizontal section at core mid-plane

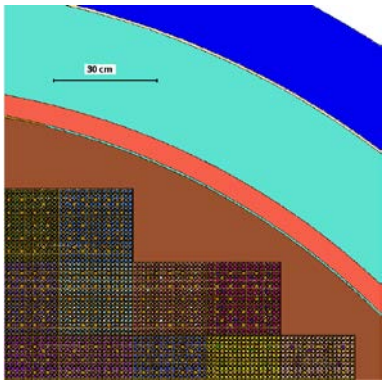

Figure 12. PWR GEN III: Horizontal section (detail)

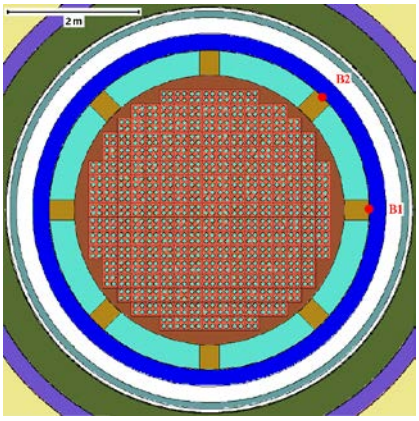

Figure 13. PWR GEN III: Horizontal section at the supporting platforms

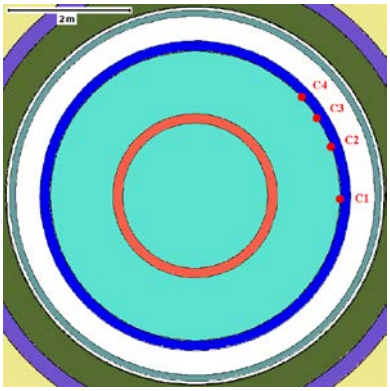

Figure 14. PWR GEN III: Horizontal section below supporting platforms

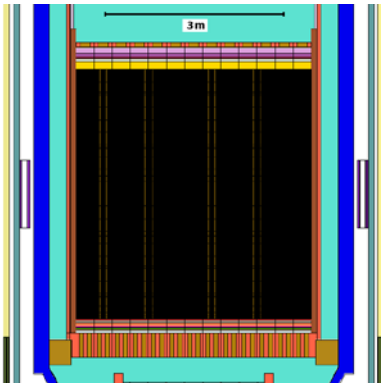

Figure 15. PWR GEN III: Vertical section showing ex-core detectors

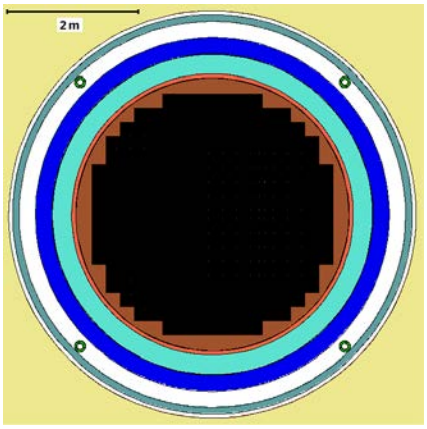

Figure 16. PWR GEN III: Horizontal section showing ex-core detectors

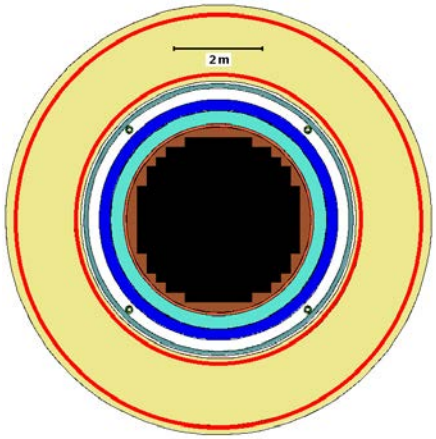

Figure 17. PWR GEN III: Horizontal section showing location of concrete activation surfaces

The series of decoupled calculations employed the fission sites as the point of decoupling and required patching MCNP with a modified *source* subroutine. The first part of the decoupled calculation was an eigenvalue calculation with no VR. Having reached the fundamental mode, 10^6 neutrons per fission generation and 120 fission generations were run. The fission sites in the appropriate spatial binning were written to a *MCTAL* file [4]. As far as the radial distribution of fission sites was concerned, a more extensive analysis was made compared with PWR GEN II. Both assembly-wise and pin-wise distributions were tested. The assembly-wise distribution mode used two axial distribution options: a single average axial distribution for all the assemblies and each assembly having its own axial distribution. The former is referred to as the “mono-axial assembly-wise description” and the latter as the “assembly-wise description” as for PWR GEN II. The pin-wise distribution mode had each pin with its own axial distribution but with two options: radially homogeneous over each pin or radially homogeneous in each of two radial bins (of equal area) in each pin (with each radial bin having its own axial distribution). The former is referred to as the “pin-wise description” and the latter as the “dual pin-wise description” as for PWR GEN II. A single axial binning was employed consisting of 52 axial bins distributed as shown in Fig. 18. The final case was a homogeneous fission source throughout the fissile volume (including cladding and water).

The energy at the point of decoupling was treated in the same way as for PWR GEN II with three possible Watt analytic fission spectra: MCNP default. ^{235}U and ^{239}Pu [4].

The responses in the first set (PV damage) were evaluated with all the spatial decoupling approximations. The ex-core detector signal was only treated with the dual pin-wise description and the homogeneous approximation. The responses in the third set were evaluated with the dual pin-wise description, the assembly-wise description (excluding the neutron dose) and the homogeneous approximation (again excluding the neutron dose).

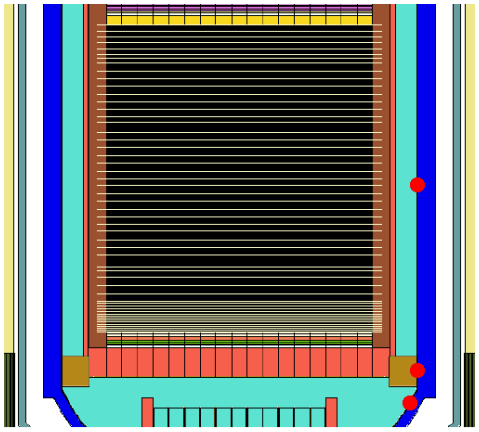

Figure 18. PWR GEN III: Axial division of fissile zone for decoupling

3.2 RESULTS

In §3.2.1 we show the absolute results obtained with the eigenvalue calculation. Then the decoupled results, including the homogeneous case, are presented as ratios relative to the eigenvalue results: §3.2.2 contains the homogeneous results and §3.2.3 the mono-axial assembly-wise results. (The assembly-wise and (single and dual) pin-wise results are given in §3.2.1 and §3.2.2 in [1].) In §3.2.4 the variation of response with energy spectrum and with the spatial description of the fission sites of the decoupled calculation is reported for all the results apart from those reported in §3.2.3 in [1]. Two standard deviation error bars are present in all the figures but may be concealed by the data points.

3.2.1 Eigenvalue results

The results obtained with the eigenvalue calculations are shown in Table I. They are normalized to 1 W of reactor power (corresponding to a fission neutron source of 8.09×10^{10} neutrons / sec[2] that assumed 7.07% decay heat). The dpa results are further normalized to 1 year (at 1 W power). The fractional standard deviation (1 fsd) is in brackets after the response.

[2] Consistently with what was done in §2.2, a +F6 tally over all in- and ex-core cells in a MCNP coupled neutron-photon calculation gave 71.73 MeV per source fission neutron. [This (prompt) energy deposition value was again just under 5% greater than the result of a F7:n tally over all in-core cells.]

Table I. PWR GEN III: results from single eigenvalue run normalized to 1 W reactor power

Response set / axial position			azimuthal position or cross-section				
			1	2	3	4	
1 - A	ϕ_n > 1 MeV	n cm^{-2} s^{-1}	0.609 (0.0050)	2.21 (0.0024)	2.78 (0.0024)	2.54 (0.0030)	
1 - B	ϕ_n > 1 MeV	n cm^{-2} s^{-1}	3.10E-3 (0.0061)	9.60E-3 (0.0052)			
1 - C	ϕ_n > 1 MeV	n cm^{-2} s^{-1}	9.13E-5 (0.0092)	5.26E-4 (0.0079)	5.61E-4 (0.0083)	1.75E-4 (0.0085)	
1 - A	ϕ_n > 100 keV	n cm^{-2} s^{-1}	1.75 (0.0050)	5.57 (0.0023)	6.87 (0.0022)	6.39 (0.0029)	
1 - B	ϕ_n > 100 keV	n cm^{-2} s^{-1}	0.139 (0.0030)	0.216 (0.0028)			
1 - C	ϕ_n > 100 keV	n cm^{-2} s^{-1}	5.92E-3 (0.0032)	6.37E-3 (0.0032)	7.03E-3 (0.0032)	7.74E-3 (0.0028)	
1 - A	dpa (n)	$year^{-1}$	3.24E-14 (0.0045)	1.08E-13 (0.0023)	1.34E-13 (0.0023)	1.23E-13 (0.0028)	
1 - B	dpa (n)	$year^{-1}$	1.19E-15 (0.0029)	1.95E-15 (0.0029)			
1 - C	dpa (n)	$year^{-1}$	4.27E-17 (0.0027)	5.81E-17 (0.0043)	6.34E-17 (0.0042)	5.68E-17 (0.0026)	
1 - A	dpa (γ)	$year^{-1}$	6.72E-15 (0.0074)	9.16E-15 (0.0046)	9.51E-15 (0.0046)	9.51E-15 (0.0064)	
1 - B	dpa (γ)	$year^{-1}$	1.31E-17 (0.0149)	1.61E-17 (0.0099)			
1 - C	dpa (γ)	$year^{-1}$	5.86E-18 (0.0211)	5.38E-17 (0.0072)	4.80E-17 (0.0109)	5.94E-18 (0.0228)	
2	$^{10}B(n,\alpha)$	cm^{-3} s^{-1}	97.3 (0.0031)				
			$^{59}Co(n,\gamma)$	$^{151}Eu(n,\gamma)$	$^{153}Eu(n,\gamma)$	$^{54}Fe(n,\gamma)$	$^{56}Fe(n,2n)$
3	15 cm depth	cm^{-3} s^{-1}	6.22E-5 (0.0008)	2.99E-5 (0.0008)	1.53E-6 (0.0008)	2.15E-3 (0.0008)	1.16E-7 (0.0092)
3	150 cm depth	cm^{-3} s^{-1}	4.69E-12 (0.0008)	2.26E-12 (0.0021)	1.13E-13 (0.0020)	1.64E-10 (0.0021)	3.60E-13 (0.0230)
			neutron dose				
3	15 cm depth	pSv	6.67 (0.0019)				
3	150 cm depth	pSv	2.23E-6 (0.0060)				

3.2.2 Homogeneous fission source results

As the homogeneous case is only useful for responses at the level of the core mid-plane or averaged over the height of the core, results will not be presented for the PV damage responses at positions B1, B2 and C1 – C4. Figs. 19 – 21 show the ratios: decoupled / eigenvalue result for the Watt fission spectrum with parameters: MCNP default, neutron-induced fission in ^{235}U and in ^{239}Pu respectively [4].

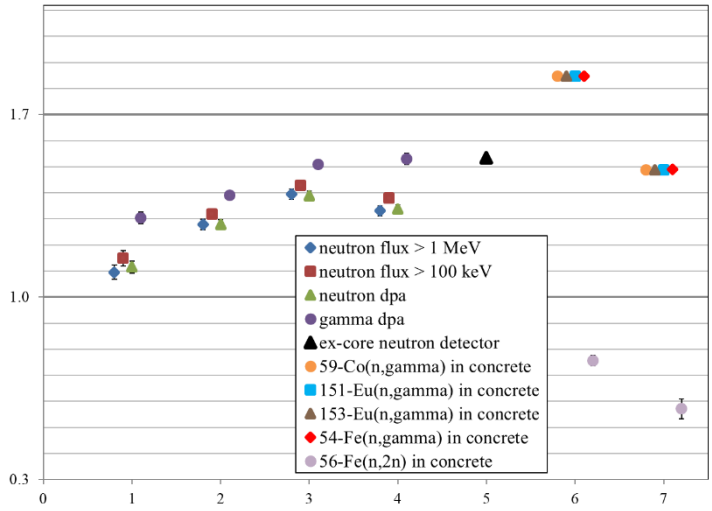

Figure 19. PWR GEN III: Ratio of decoupled to eigenvalue result for the MCNP default Watt fission spectrum and a homogeneous spatial distribution of fission sites (x: 1–4: A1–A4 in Fig. 11; 5: ex-core detector; 6, 7: concrete shielding at 15, 150 cm depth)

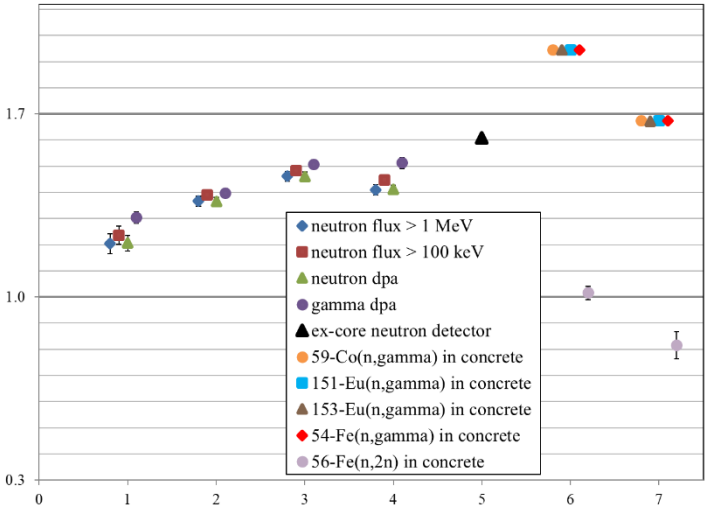

Figure 20. PWR GEN III: Ratio of decoupled to eigenvalue result for the Watt spectrum for thermal neutron-induced fission on 235U and a homogeneous spatial distribution of fission sites (x: 1– 4: A1–A4 in Fig. 11; 5: ex-core detector; 6, 7: concrete shielding at 15, 150 cm depth)

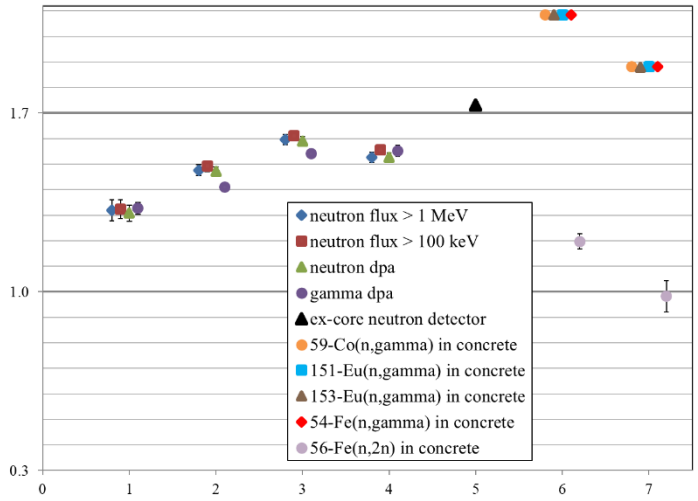

Figure 21. PWR GEN III: Ratio of decoupled to eigenvalue result for the Watt spectrum for thermal neutron-induced fission on 239Pu and a homogeneous spatial distribution of fission sites (x: 1– 4: A1–A4 in Fig. 11; 5: ex-core detector; 6, 7: concrete shielding at 15, 150 cm depth)

We see in Figs. 19 – 21 an overestimate of the response due to the spatial approximation of the fission sites. Such overestimate increases going outwards until instead at 150 cm depth in concrete it decreases presumably due to spectral considerations. Such spectral considerations are also responsible for the difference between the (n,γ) and the (n,2n) reaction rates. As for the PWR GEN II model, the ratio increases going from the default to the ^{235}U to the ^{239}Pu spectrum.

3.2.3 Mono-axial assembly-wise fission source results

This approximation was only employed for the PV damage responses. Figs. 22 – 24 show the ratios: decoupled / eigenvalue result for the Watt fission spectrum with parameters: MCNP default, neutron-induced fission in ^{235}U and in ^{239}Pu respectively. We see in these figures that for all three spectra the approximation overestimates the results at the core mid-plane. At and below the support platforms the results are rather noisy. However the neutron fluxes above 100 keV and the neutron and gamma dpa look also to be overestimates at these positions.

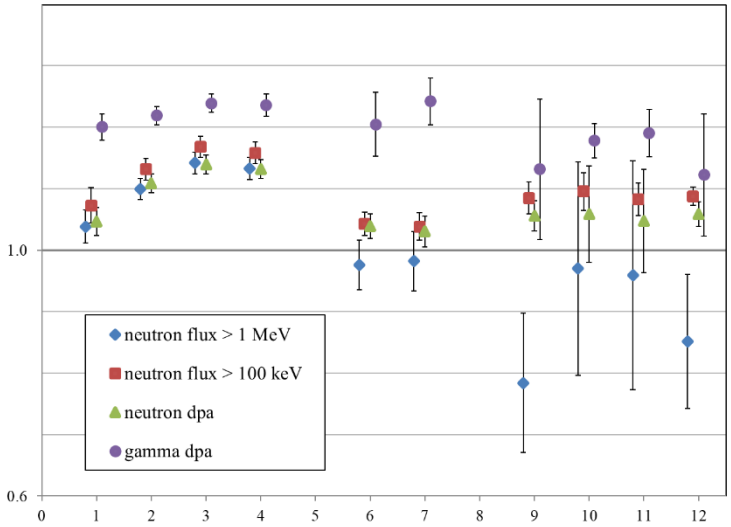

Figure 22. PWR GEN III: Ratio of decoupled to eigenvalue result for the MCNP default Watt fission spectrum and the mono-axial assembly-wise description of fission sites (x: 1–4: A1–A4 in Fig. 11; 6, 7: B1, B2 in Fig. 13; 9–12: C1–C4 in Fig. 14)

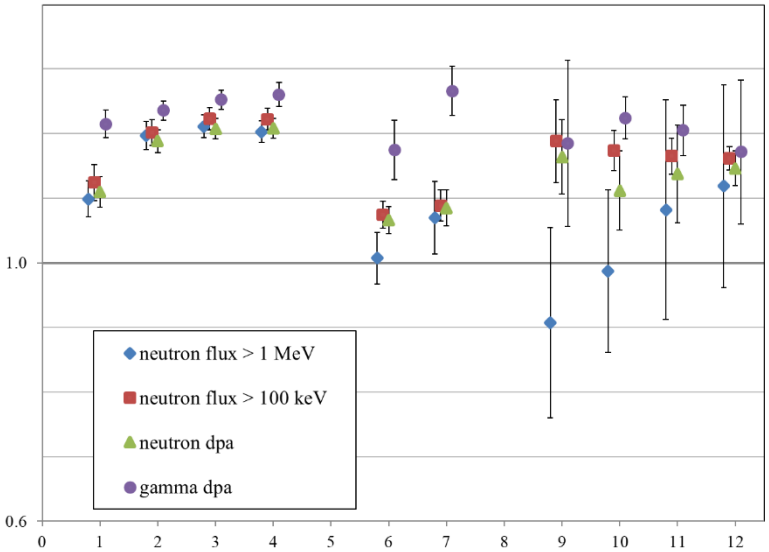

Figure 23. PWR GEN III: Ratio of decoupled to eigenvalue result for the Watt spectrum for thermal neutron-induced fission on 235U and the mono-axial assembly-wise description of fission sites (x: 1–4: A1–A4 in Fig. 11; 6, 7: B1, B2 in Fig. 13; 9–12: C1–C4 in Fig. 14)

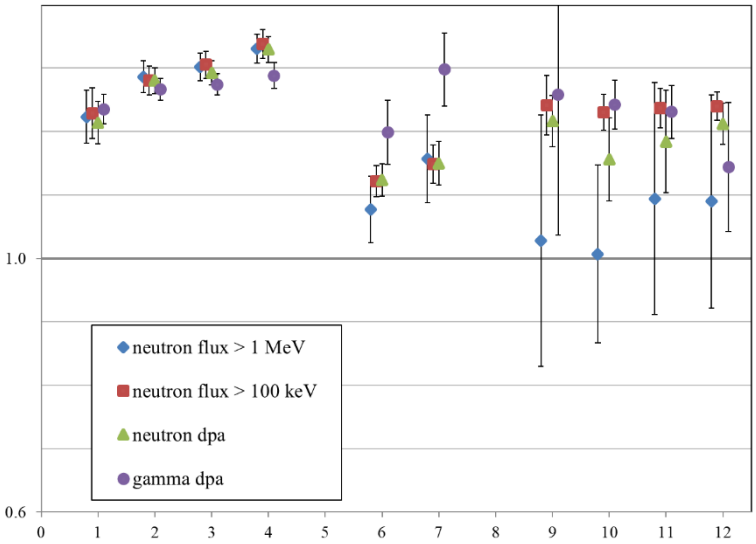

Figure 24. PWR GEN III: Ratio of decoupled to eigenvalue result for the Watt spectrum for thermal neutron-induced fission on 239Pu and the mono-axial assembly-wise description of fission sites (x: 1–4: A1–A4 in Fig. 11; 6, 7: B1, B2 in Fig. 13; 9–12: C1–C4 in Fig. 14)

3.2.4 Decoupled response with energy spectrum and spatial description

The subset of the responses whose results were already reported in §3.2.3 in [1] consisted of all four damage responses at positions A3, B2 and C1, the ex-core neutron detectors and the ^{151}Eu(n,γ) rate at both depths in the concrete. Here we report all four damage responses at the remaining positions A1, A2, A4 (Fig. 11), B1 (Fig. 13), C2, C3, C4 (Fig. 14) and the remaining activation rates at 15 and 150 cm depth in the concrete (Fig. 17): ^{59}Co(n,γ), ^{153}Eu(n,γ), ^{54}Fe(n,γ), ^{56}Fe(n,2n), plus the neutron dose rate [5].

3.2.4.1 Energy Spectrum

We only consider here the dual pin-wise description of the fission sites. Figs. 25-1 – 25-7 show the variation with energy spectrum of the ratios: decoupled / eigenvalue result for the PV damage responses at the positions A1, A2, A4, B1. C2, C3 and C4 respectively.

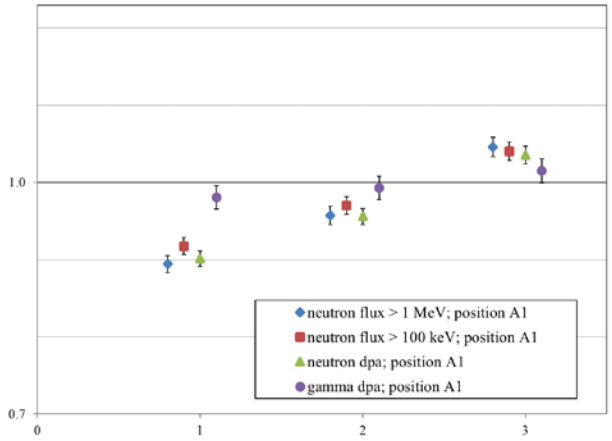

Fig. 25-1. position A1

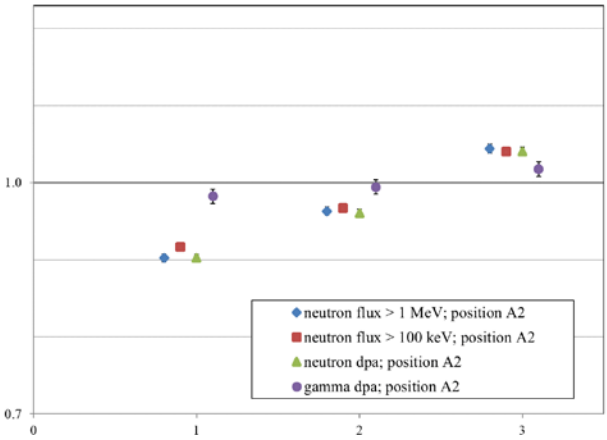

Fig. 25-2. position A2

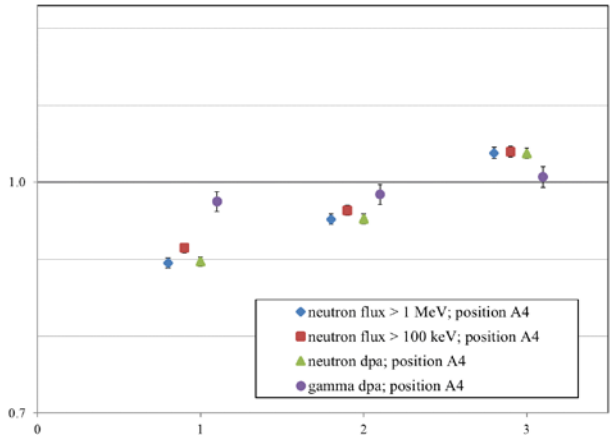

Fig. 25-3. position A4

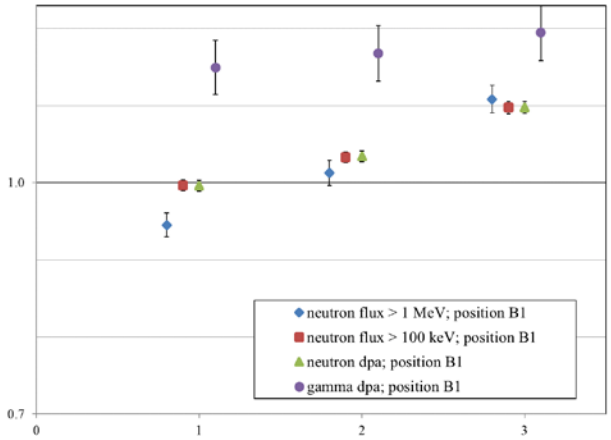

Fig. 25-4. position B1

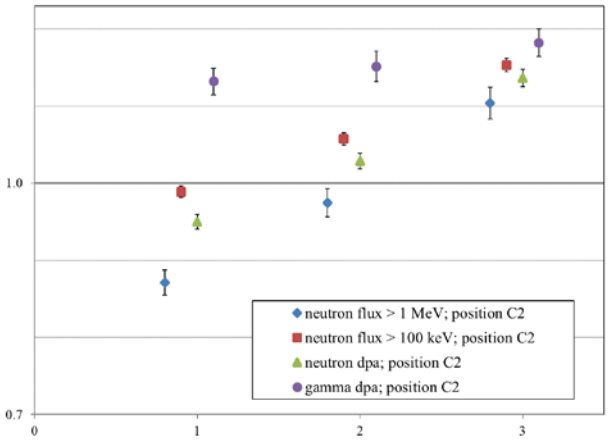

Fig. 25-5. position C2

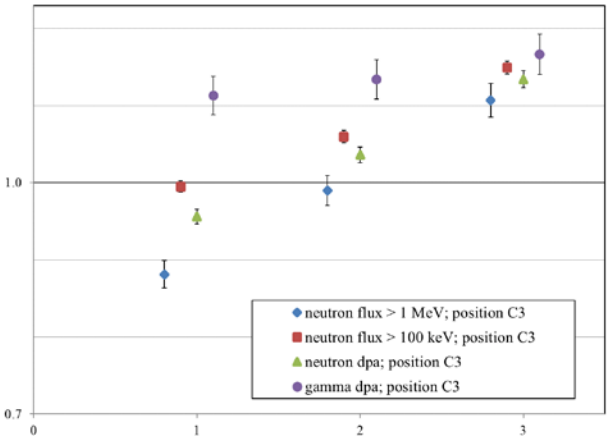

Fig. 25-6. position C3

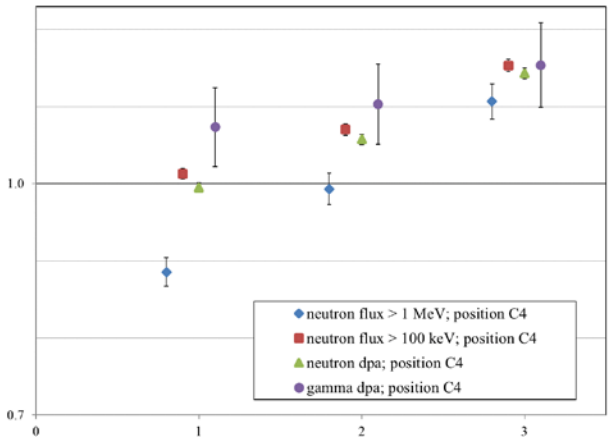

Fig. 25-7. position C4

Figures 25-1, 25-2, 25-3, 25-4, 25-5, 25-6 and 25-7. PWR GEN III: Ratio of decoupled to eigenvalue result for the dual pin-wise description of fission sites, at positions A1, A2, A4, B1, C2, C3 and C4, for Watt fission spectra with various parameters (x: 1: MCNP default; 2: thermal neutron-induced in 235U; 3: thermal neutron-induced in 239Pu)

Exactly the same remarks can be made concerning the results in Figs. 25 as were made

concerning the results at positions A3, B2 and C1: Figs. 33-1, 33-2 and 33-3 in [1], and will not be repeated here.

Figs. 26-1 – 26-4 show the variation with energy spectrum of the ratios: decoupled / eigenvalue result for the ^{59}Co(n,γ), ^{153}Eu(n,γ), ^{54}Fe(n,γ) and ^{56}Fe(n,2n) reaction rates and the neutron dose rate at 15 and 150 cm depths in the concrete.

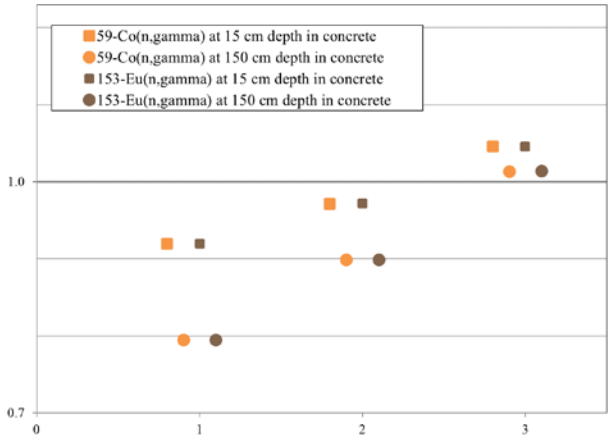

Fig. 26-1. 59Co(n, γ) and 153Eu(n, γ) rates

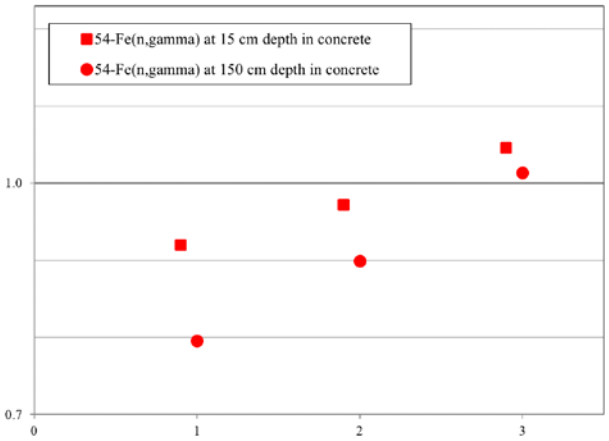

Fig. 26-2. 54Fe(n, γ) rate

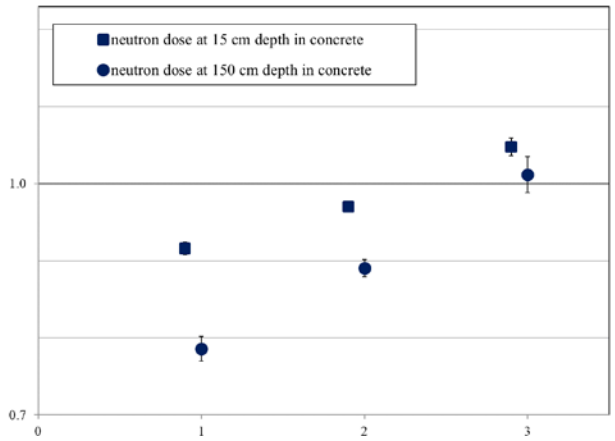

Fig. 26-3. neutron dose rate

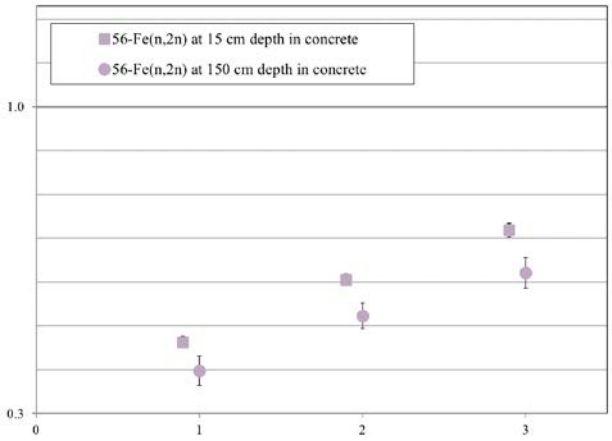

Fig. 26-4. 56Fe(n,2n) rate

Figures 26-1, 26-2, 26-3 and 26-4. PWR GEN III: Ratio of decoupled to eigenvalue result for the dual pin-wise description of fission sites, for the 59Co(n, γ), 153Eu(n, γ), 54Fe(n, γ) and 56Fe(n,2n) reaction rates and the neutron dose rate at 15 and 150 cm depths in the concrete, for Watt fission spectra with various parameters (x: 1: MCNP default; 2: thermal neutron-induced in 235U; 3: thermal neutron-induced in 239Pu)

In Figs. 26-1 – 26-3 we see a steeper gradient at 150 cm depth compared with 15 cm depth, as was noted also concerning Fig. 33-4 in [1]. Fig. 26-4 has a different scale and a slightly different behaviour from the other Figs. 25 and 26 (and from Figs. 33 in [1]). We remind ourselves that the threshold for this cross-section is around 11.5 MeV.

3.2.4.2 Spatial Description

The triplets: Figs. 27 – 29, 30 – 32, 33 – 35, 36 – 38, 39 – 41, 42 – 44 and 45 – 47 show the variation with spatial approximation of the ratios: decoupled / eigenvalue result for the PV damage responses at positions A1, A2, A4, B1. C2, C3 and C4 respectively. Within each triplet, the energy spectrum of the source in the second part of the decoupled calculation is described by the Watt fission spectrum with parameters: MCNP default, neutron-induced fission in ^{235}U and in ^{239}Pu respectively.

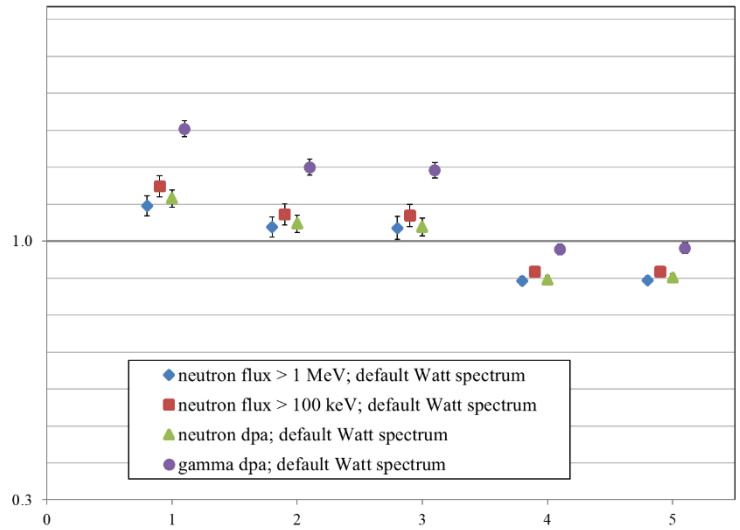

Figure 27. PWR GEN III: Ratio of decoupled to eigenvalue result at position A1 for the MCNP default Watt fission spectrum and following spatial binning of the fission sites (x: 1: homogeneous; 2: mono-axial assembly-wise; 3: assembly-wise; 4: pin-wise; 5: dual pin-wise)

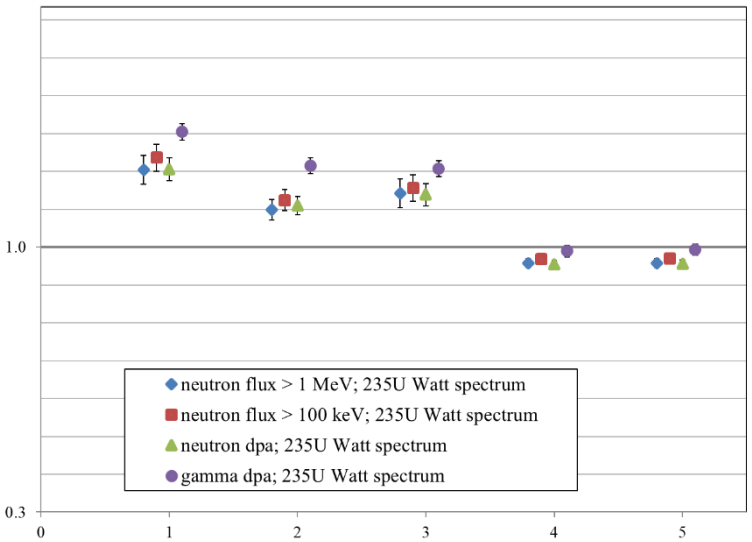

Figure 28. PWR GEN III: Ratio of decoupled to eigenvalue result at position A1 for the Watt spectrum for thermal neutron-induced fission on 235U and following spatial binning of the fission sites (x: 1: homogeneous; 2: mono-axial assembly-wise; 3: assembly-wise; 4: pin-wise; 5: dual pin-wise)

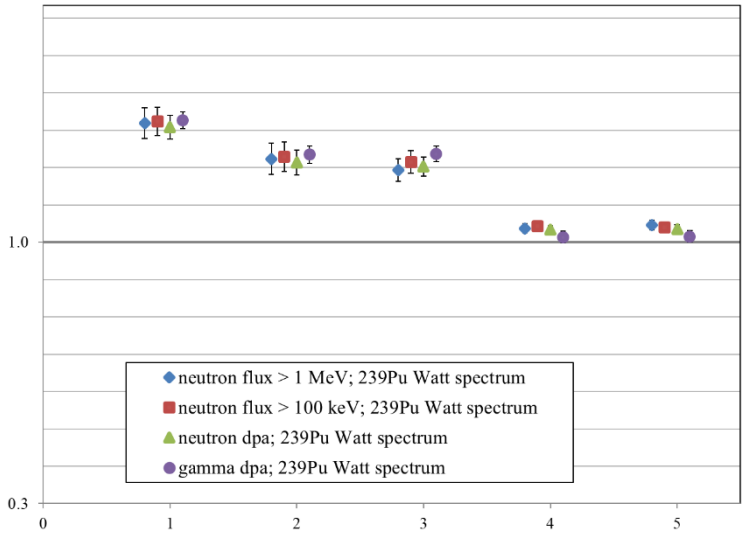

Figure 29. PWR GEN III: Ratio of decoupled to eigenvalue result at position A1 for the Watt spectrum for thermal neutron-induced fission on 239Pu and following spatial binning of the fission sites (x: 1: homogeneous; 2: mono-axial assembly-wise; 3: assembly-wise; 4: pin-wise; 5: dual pin-wise)

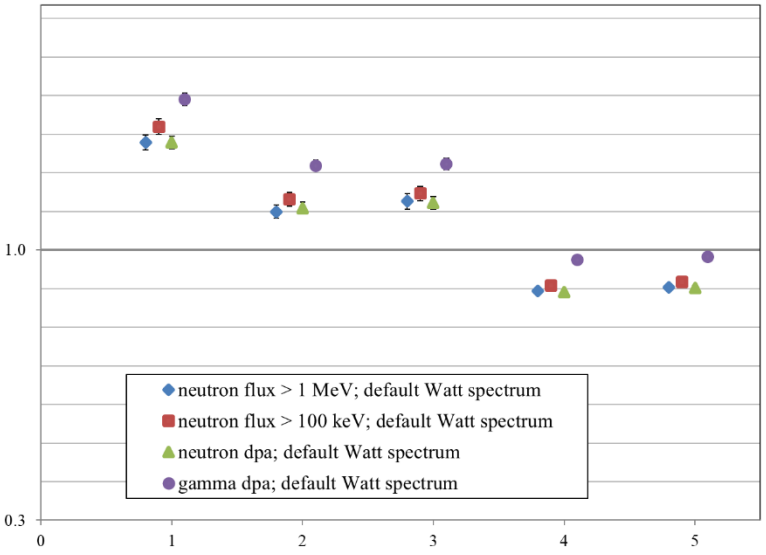

Figure 30. PWR GEN III: Ratio of decoupled to eigenvalue result at position A2 for the MCNP default Watt fission spectrum and following spatial binning of the fission sites (x: 1: homogeneous; 2: mono-axial assembly-wise; 3: assembly-wise; 4: pin-wise; 5: dual pin-wise)

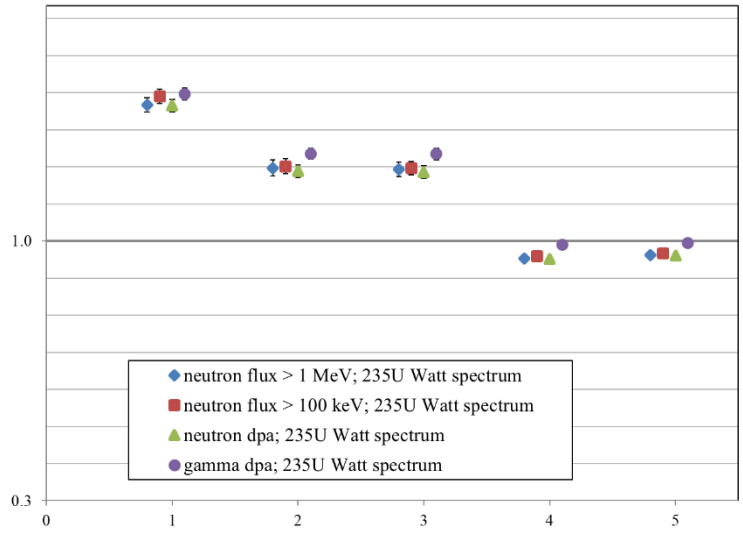

Figure 31. PWR GEN III: Ratio of decoupled to eigenvalue result at position A2 for the Watt spectrum for thermal neutron-induced fission on 235U and following spatial binning of the fission sites (x: 1: homogeneous; 2: mono-axial assembly-wise; 3: assembly-wise; 4: pin-wise; 5: dual pin-wise)

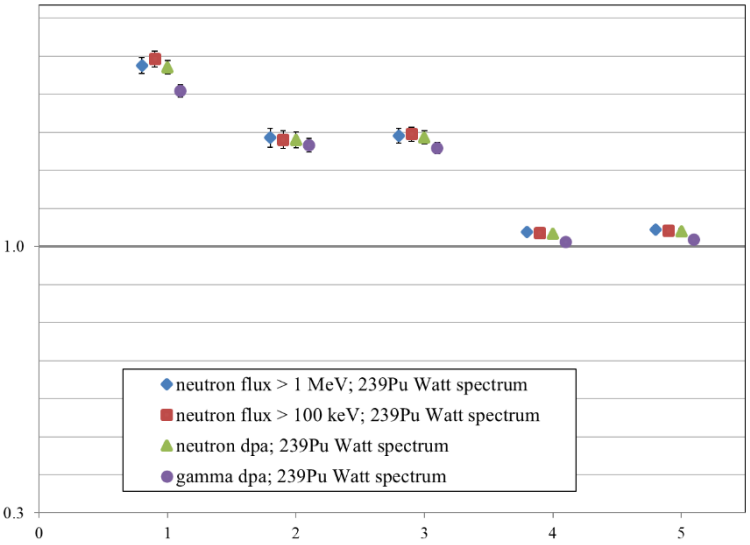

Figure 32. PWR GEN III: Ratio of decoupled to eigenvalue result at position A2 for the Watt spectrum for thermal neutron-induced fission on 239Pu and following spatial binning of the fission sites (x: 1: homogeneous; 2: mono-axial assembly-wise; 3: assembly-wise; 4: pin-wise; 5: dual pin-wise)

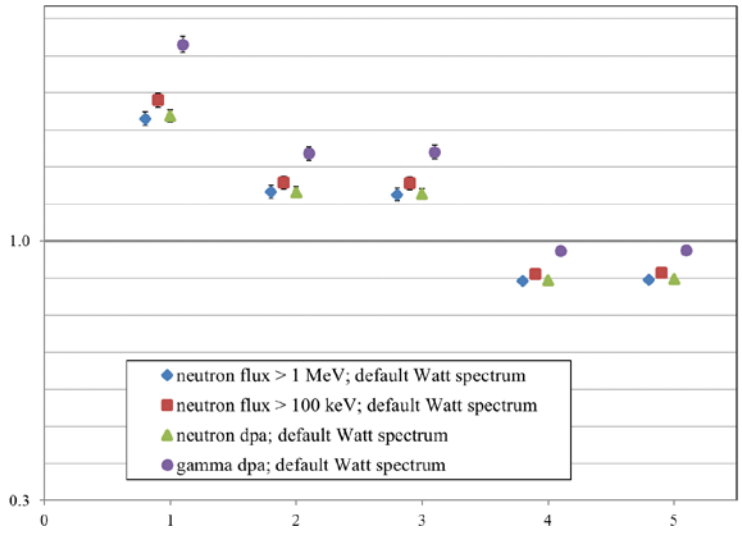

Figure 33. PWR GEN III: Ratio of decoupled to eigenvalue result at position A4 for the MCNP default Watt fission spectrum and following spatial binning of the fission sites (x: 1: homogeneous; 2: mono-axial assembly-wise; 3: assembly-wise; 4: pin-wise; 5: dual pin-wise)

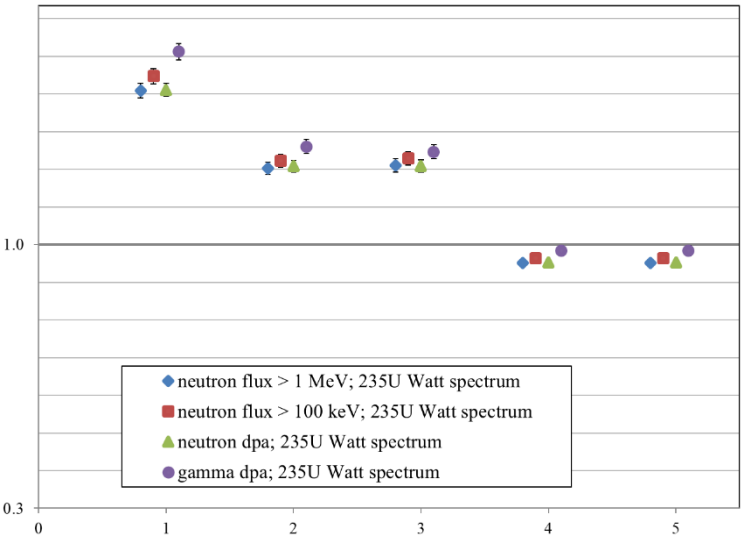

Figure 34. PWR GEN III: Ratio of decoupled to eigenvalue result at position A4 for the Watt spectrum for thermal neutron-induced fission on 235U and following spatial binning of the fission sites (x: 1: homogeneous; 2: mono-axial assembly-wise; 3: assembly-wise; 4: pin-wise; 5: dual pin-wise)

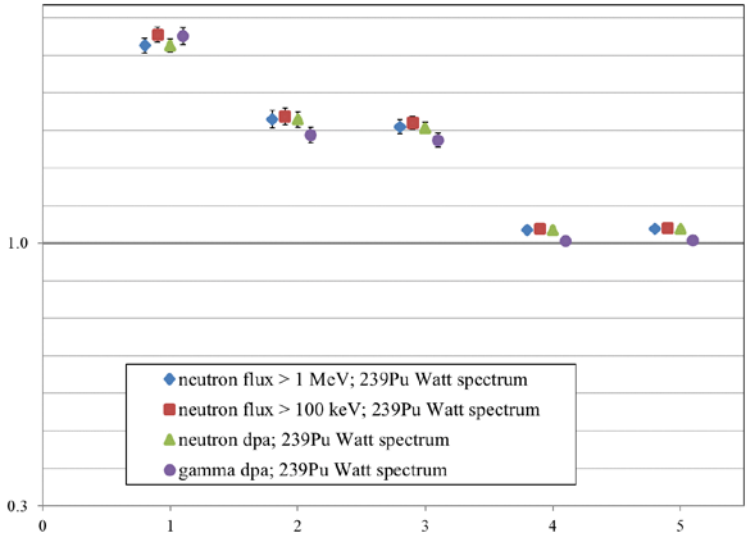

Figure 35. PWR GEN III: Ratio of decoupled to eigenvalue result at position A4 for the Watt spectrum for thermal neutron-induced fission on 239Pu and following spatial binning of the fission sites (x: 1: homogeneous; 2: mono-axial assembly-wise; 3: assembly-wise; 4: pin-wise; 5: dual pin-wise)

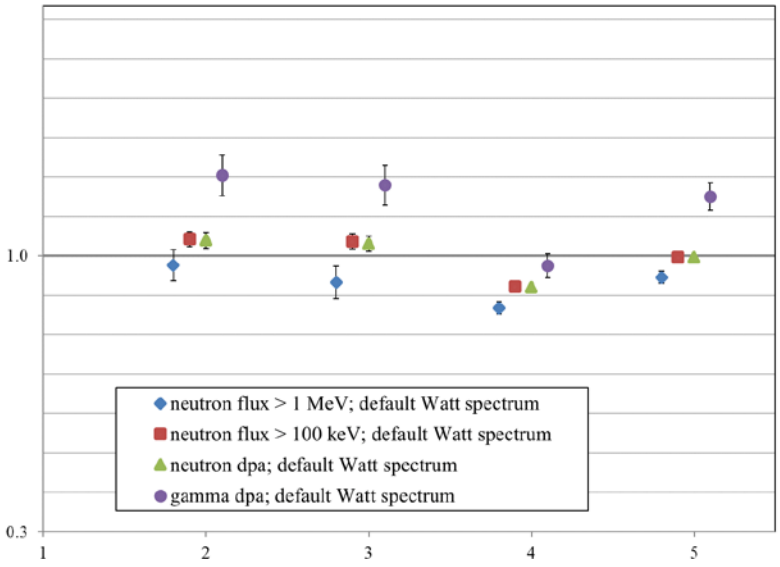

Figure 36. PWR GEN III: Ratio of decoupled to eigenvalue result at position B1 for the MCNP default Watt fission spectrum and following spatial binning of the fission sites (x: 2: mono-axial assembly-wise; 3: assembly-wise; 4: pin-wise; 5: dual pin-wise)

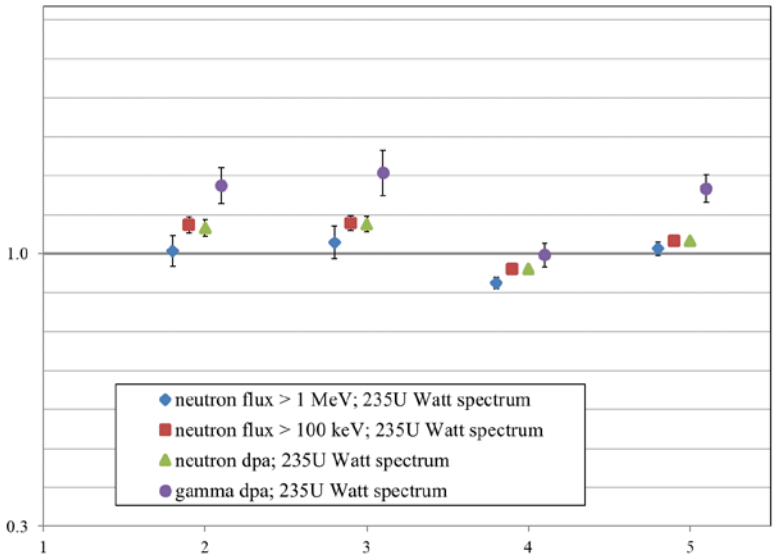

Figure 37. PWR GEN III: Ratio of decoupled to eigenvalue result at position B1 for the Watt spectrum for thermal neutron-induced fission on 235U and following spatial binning of the fission sites (x: 2: mono-axial assembly-wise; 3: assembly-wise; 4: pin-wise; 5: dual pin-wise)

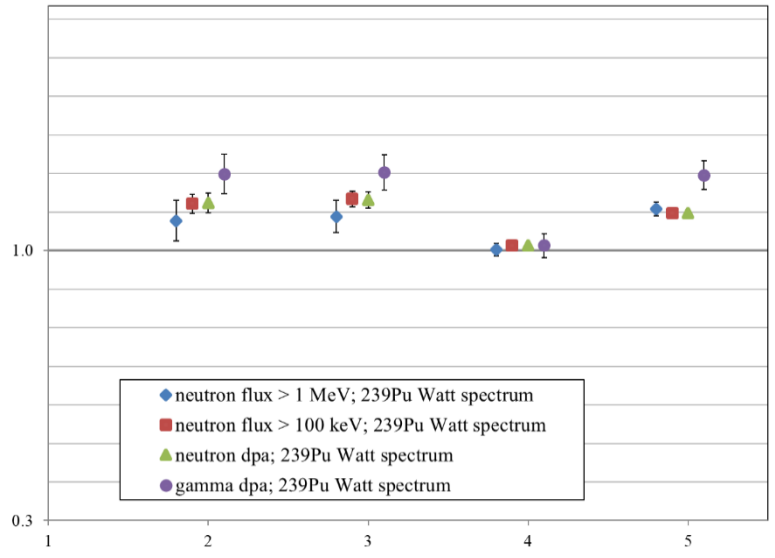

Figure 38. PWR GEN III: Ratio of decoupled to eigenvalue result at position B1 for the Watt spectrum for thermal neutron-induced fission on 239Pu and following spatial binning of the fission sites (x: 2: mono-axial assembly-wise; 3: assembly-wise; 4: pin-wise; 5: dual pin-wise)

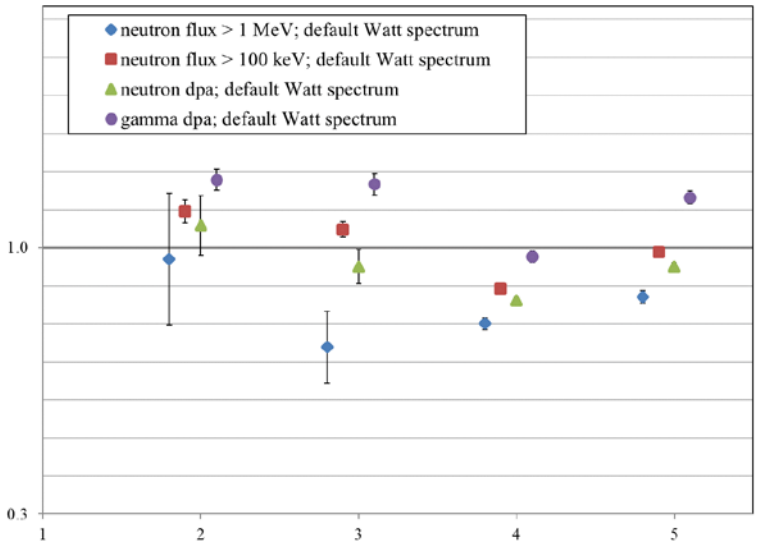

Figure 39. PWR GEN III: Ratio of decoupled to eigenvalue result at position C2 for the MCNP default Watt fission spectrum and following spatial binning of the fission sites (x: 2: mono-axial assembly-wise; 3: assembly-wise; 4: pin-wise; 5: dual pin-wise)

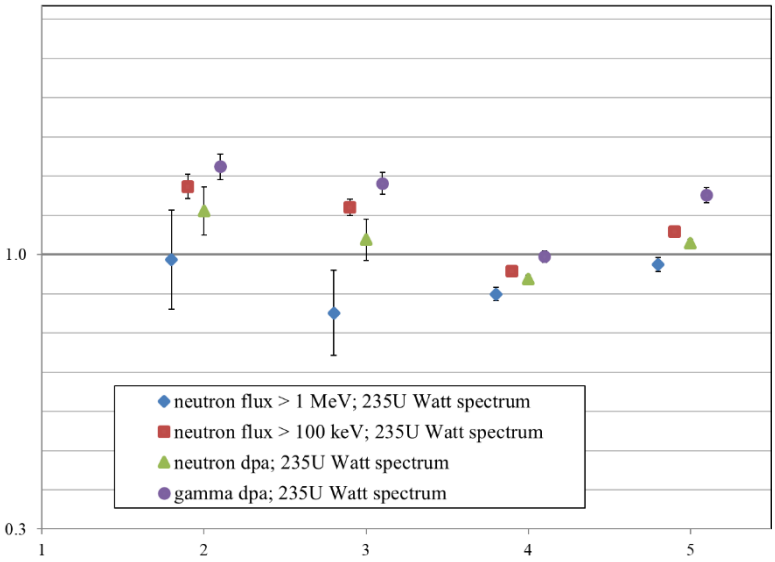

Figure 40. PWR GEN III: Ratio of decoupled to eigenvalue result at position C2 for the Watt spectrum for thermal neutron-induced fission on 235U and following spatial binning of the fission sites (x: 2: mono-axial assembly-wise; 3: assembly-wise; 4: pin-wise; 5: dual pin-wise)

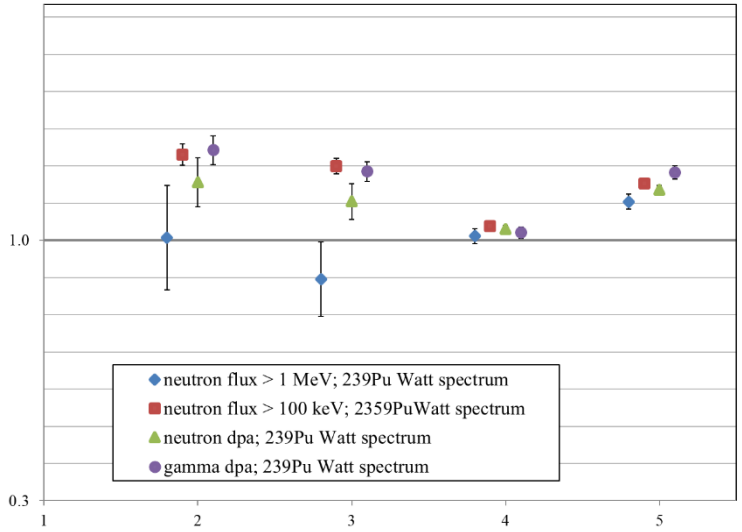

Figure 41. PWR GEN III: Ratio of decoupled to eigenvalue result at position C2 for the Watt spectrum for thermal neutron-induced fission on 239Pu and following spatial binning of the fission sites (x: 2: mono-axial assembly-wise; 3: assembly-wise; 4: pin-wise; 5: dual pin-wise)

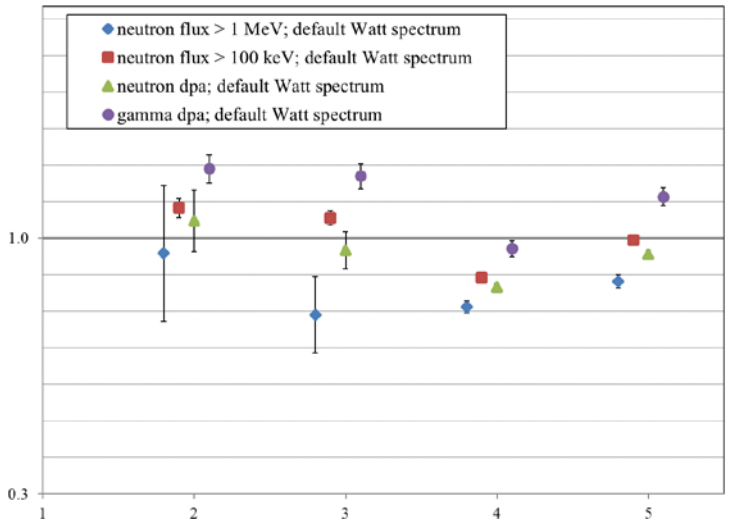

Figure 42. PWR GEN III: Ratio of decoupled to eigenvalue result at position C3 for the MCNP default Watt fission spectrum and following spatial binning of the fission sites (x: 2: mono-axial assembly-wise; 3: assembly-wise; 4: pin-wise; 5: dual pin-wise)

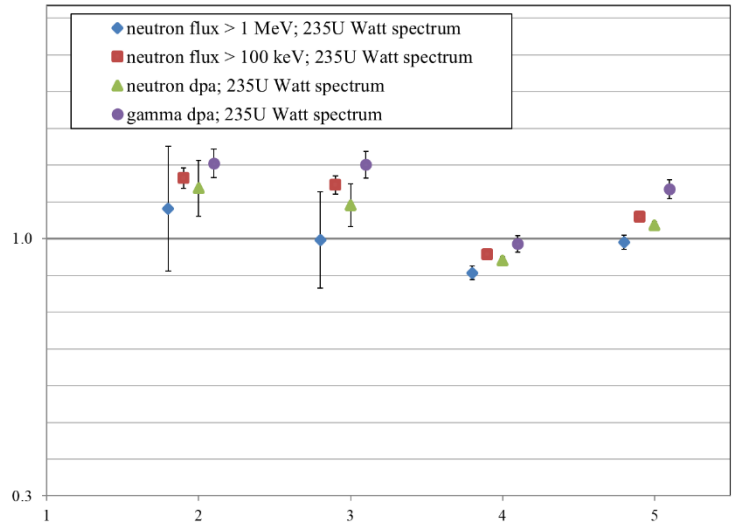

Figure 43. PWR GEN III: Ratio of decoupled to eigenvalue result at position C3 for the Watt spectrum for thermal neutron-induced fission on 235U and following spatial binning of the fission sites (x: 2: mono-axial assembly-wise; 3: assembly-wise; 4: pin-wise; 5: dual pin-wise)

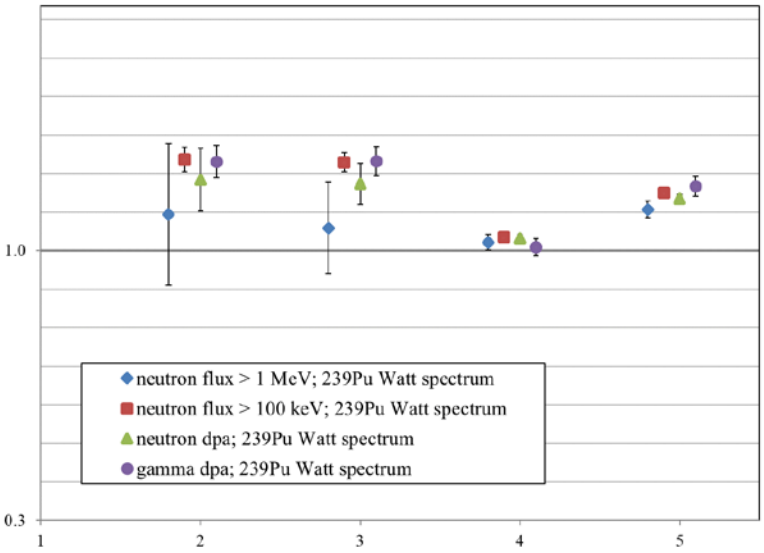

Figure 44. PWR GEN III: Ratio of decoupled to eigenvalue result at position C3 for the Watt spectrum for thermal neutron-induced fission on 239Pu and following spatial binning of the fission sites (x: 2: mono-axial assembly-wise; 3: assembly-wise; 4: pin-wise; 5: dual pin-wise)

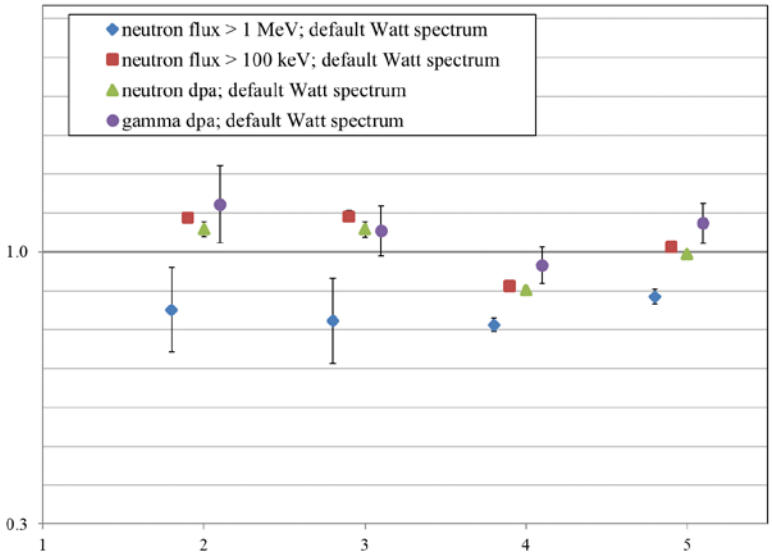

Figure 45. PWR GEN III: Ratio of decoupled to eigenvalue result at position C4 for the MCNP default Watt fission spectrum and following spatial binning of the fission sites (x: 2: mono-axial assembly-wise; 3: assembly-wise; 4: pin-wise; 5: dual pin-wise)

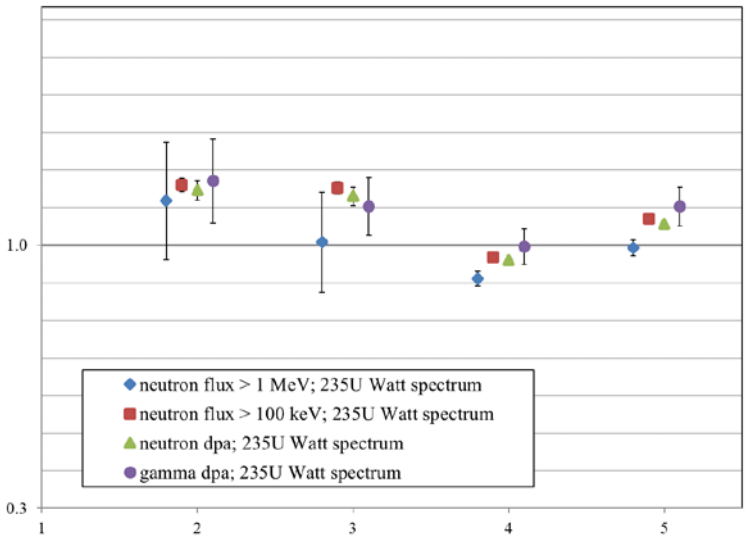

Figure 46. PWR GEN III: Ratio of decoupled to eigenvalue result at position C4 for the Watt spectrum for thermal neutron-induced fission on 235U and following spatial binning of the fission sites (x: 2: mono-axial assembly-wise; 3: assembly-wise; 4: pin-wise; 5: dual pin-wise)

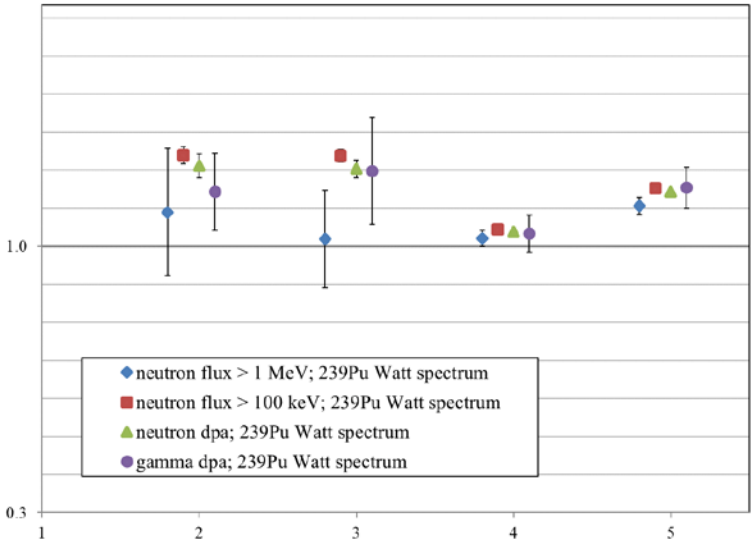

Figure 47. PWR GEN III: Ratio of decoupled to eigenvalue result at position C4 for the Watt spectrum for thermal neutron-induced fission on 239Pu and following spatial binning of the fission sites (x: 2: mono-axial assembly-wise; 3: assembly-wise; 4: pin-wise; 5: dual pin-wise)

Concerning the results in Figs. 27 – 47, the comments in §3.2.3.2 in [1] concerning the results at positions A3, B2 and C1 may be transposed here with just one *caveat*:

- For positions A1, A2 and A4, the two assembly-wise models are situated, rather than ½ way between the homogeneous model and the two pin-wise models, in most cases nearer the homogeneous model than the two pin-wise models.

The triplets: Figs. 48 – 50, 51 – 53 and 54 – 56 show the variation with spatial approximation of the ratios: decoupled / eigenvalue result for the ^{59}Co(n,γ) and ^{153}Eu(n,γ) reaction rates, the ^{54}Fe(n,γ) reaction rate and the ^{56}Fe(n,2n) reaction rate respectively at 15 and 150 cm depths in the concrete. Within each triplet, the energy spectrum of the source in the second part of the decoupled calculation is described by the Watt fission spectrum with parameters: MCNP default, neutron-induced fission in ^{235}U and in ^{239}Pu respectively. (Note that the neutron dose response in the concrete does not appear in these figures as it was evaluated with only one spatial approximation: the dual pin-wise model. The results are shown in Figs. 27 – 29 in [1] and in Fig. 26-3 above.)

Concerning the results in Figs. 48 – 56, as commented in §3.2.3.2 in [1] for the results of the ^{151}Eu(n,γ) reaction rate, the assembly-wise model is nearer to the dual pin-wise model and farther from the homogeneous approximation. The ^{56}Fe(n,2n) results in Figs. 54 – 56 are lower than the ^{59}Co(n,γ), ^{153}Eu(n,γ) and ^{54}Fe(n,γ) results in Figs. 48 – 53 for reasons discussed in §4.1 in [1]. Also the gradient: homogeneous – assembly-wise – dual pin-wise of ^{56}Fe(n,2n) is lower than the other reaction rates, presumably reflecting the penetrating ability in the core of the neutrons in the high energy tail of the fission distribution.

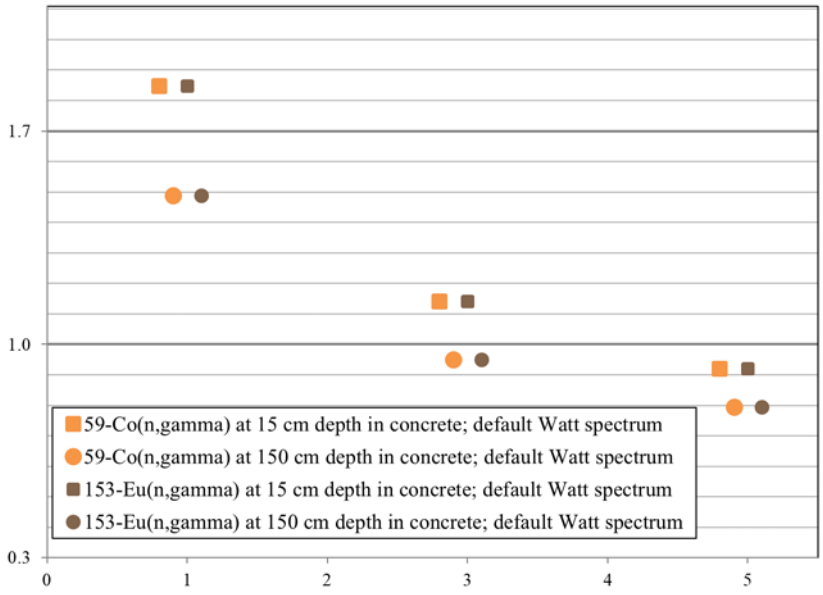

Figure 48. PWR GEN III: Ratio of decoupled to eigenvalue result for the 59Co(n, γ) and 153Eu(n, γ) rates in the concrete for the MCNP default Watt fission spectrum and following spatial binning of the fission sites (x: 1: homogeneous; 3: assembly-wise; 5: dual pin-wise)

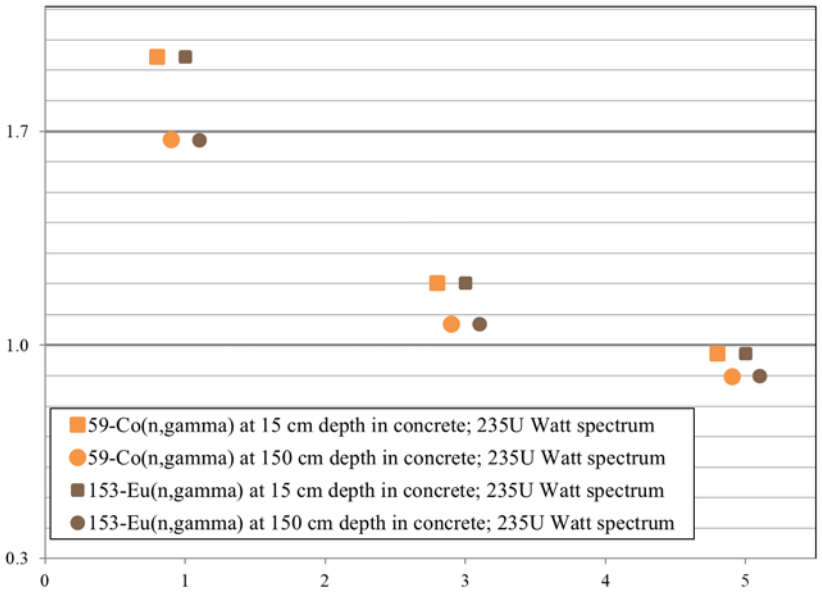

Figure 49. PWR GEN III: Ratio of decoupled to eigenvalue result for the 59Co(n, γ) and 153Eu(n, γ) rates in the concrete for the Watt spectrum for thermal neutron-induced fission on 235U and following spatial binning of the fission sites (x: 1: homogeneous; 3: assembly-wise; 5: dual pin-wise)

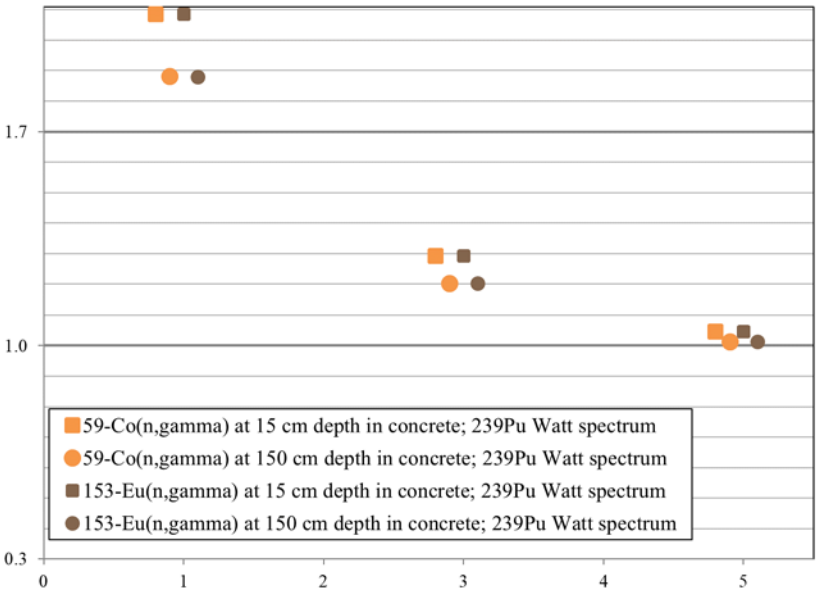

Figure 50. PWR GEN III: Ratio of decoupled to eigenvalue result for the 59Co(n, γ) and 153Eu(n, γ) rates in the concrete for the Watt spectrum for thermal neutron-induced fission on 239Pu and following spatial binning of the fission sites (x: 1: homogeneous; 3: assembly-wise; 5: dual pin-wise)

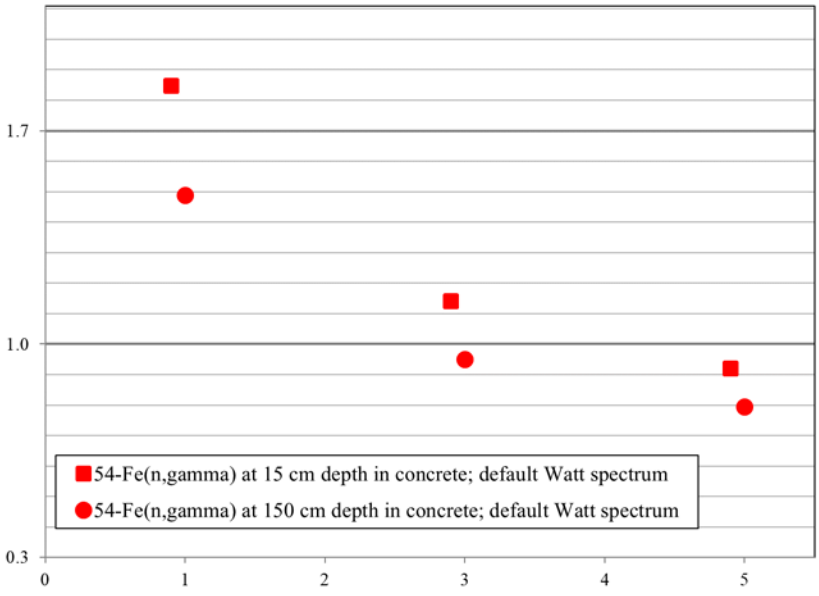

Figure 51. PWR GEN III: Ratio of decoupled to eigenvalue result for the 54Fe(n, γ) rate in the concrete for the MCNP default Watt fission spectrum and following spatial binning of the fission sites (x: 1: homogeneous; 3: assembly-wise; 5: dual pin-wise)

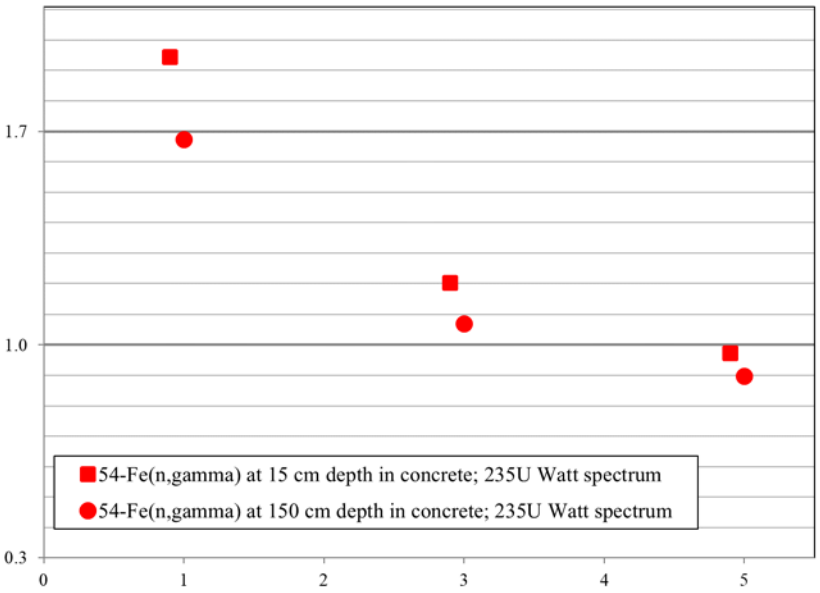

Figure 52. PWR GEN III: Ratio of decoupled to eigenvalue result for the 54Fe(n, γ) rate in the concrete for the Watt spectrum for thermal neutron-induced fission on 235U and following spatial binning of the fission sites (x: 1: homogeneous; 3: assembly-wise; 5: dual pin-wise)

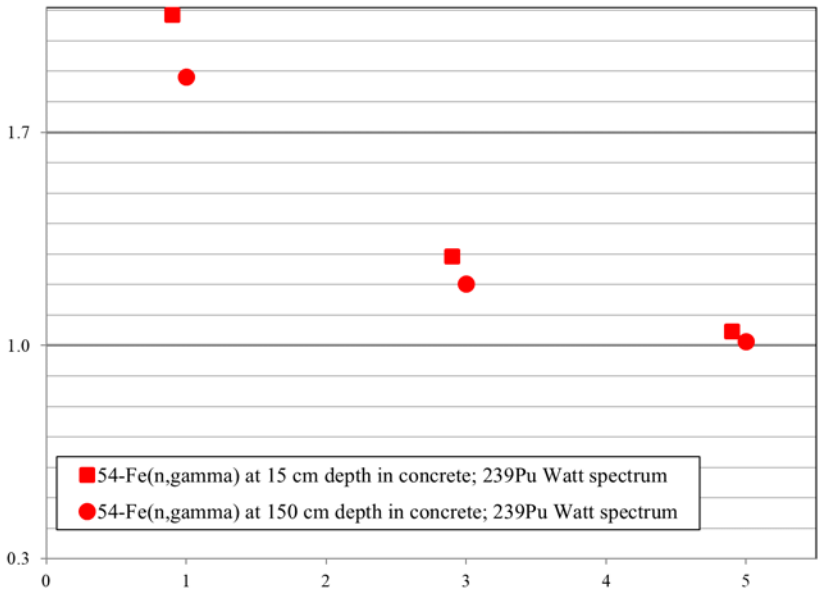

Figure 53. PWR GEN III: Ratio of decoupled to eigenvalue result for the 54Fe(n, γ) rate in the concrete for the Watt spectrum for thermal neutron-induced fission on 239Pu and following spatial binning of the fission sites (x: 1: homogeneous; 3: assembly-wise; 5: dual pin-wise)

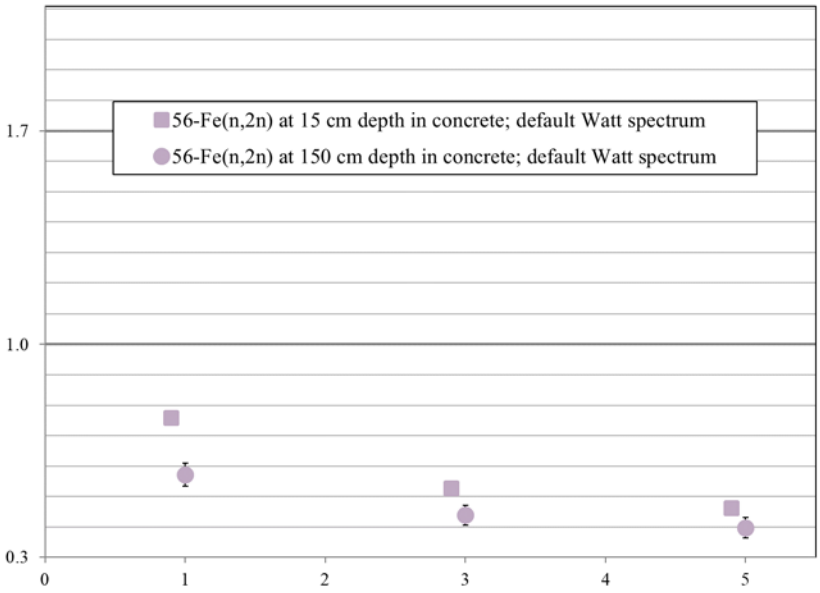

Figure 54. PWR GEN III: Ratio of decoupled to eigenvalue result for the 56Fe(n,2n) rate in the concrete for the MCNP default Watt fission spectrum and following spatial binning of the fission sites (x: 1: homogeneous; 3: assembly-wise; 5: dual pin-wise)

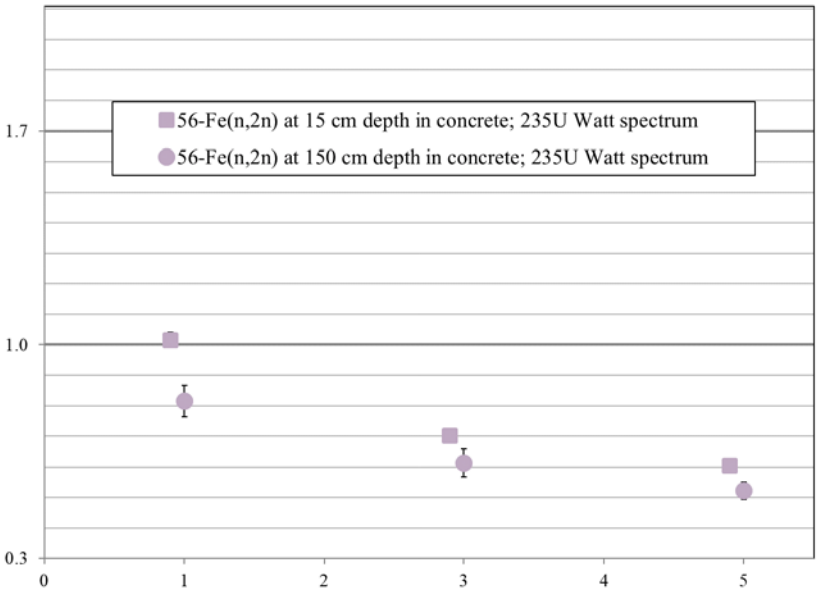

Figure 55. PWR GEN III: Ratio of decoupled to eigenvalue result for the 56Fe(n,2n) rate in the concrete for the Watt spectrum for thermal neutron-induced fission on 235U and following spatial binning of the fission sites (x: 1: homogeneous; 3: assembly-wise; 5: dual pin-wise)

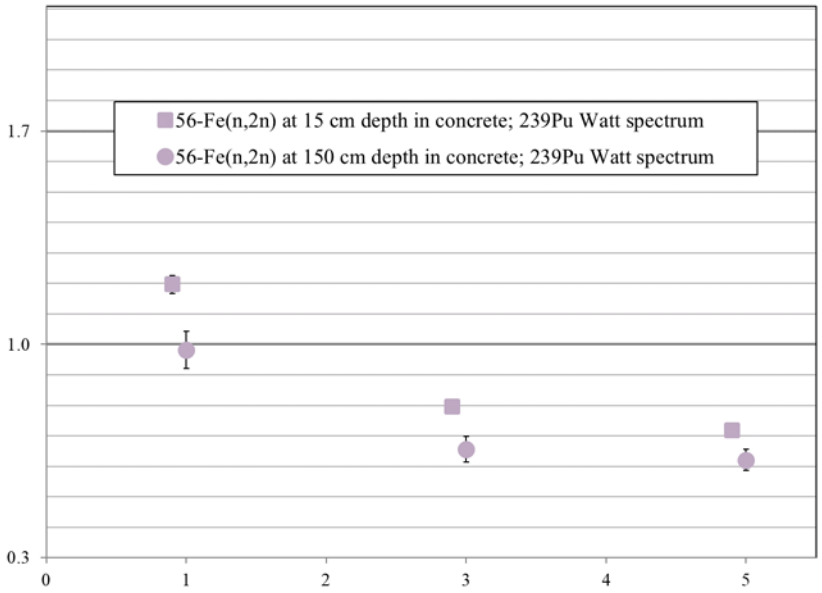

Figure 56. PWR GEN III: Ratio of decoupled to eigenvalue result for the 56Fe(n,2n) rate in the concrete for the Watt spectrum for thermal neutron-induced fission on 239Pu and following spatial binning of the fission sites (x: 1: homogeneous; 3: assembly-wise; 5: dual pin-wise)

4. CONCLUDING REMARKS

The results in this paper provide support and background to those in the article [1]. Most discussion and analysis of the results is confined to [1]. We restrict ourselves to mentioning that the results here back the conclusions drawn in [1].

ACKNOWLEDGMENTS

The computing resources and the related technical support used for this work have been provided by CRESCO/ENEAGRID High Performance Computing infrastructure and its staff. CRESCO/ENEAGRID High Performance Computing infrastructure is funded by ENEA, the Italian National Agency for New Technologies, Energy and Sustainable Economic Development and by Italian and European research programmes, see http://www.cresco.enea.it/english for information.

Dedication

This paper is dedicated to the memory of Arie Dubi (1944–2015), the originator of the DSA and a pioneering Monte Carlo developer.

REFERENCES

1. M. Brovchenko, K.W. Burn and P. Console Camprini, “On Integrating Monte Carlo Calculations in and around Near-Critical Configurations – II. Pressurized Water Reactors,” accepted for publication in Ann. Nucl. Energy (2022)
2. M. Brovchenko, K.W. Burn and P. Console Camprini, “On Integrating Monte Carlo Calculations in and around Near-Critical Configurations – I. Methodology,” Ann. Nucl. Energy 172 (2022) 109063
3. R.J. Brissenden and A.R. Garlick, “Biases in the Estimation of Keff and Its Error by Monte Carlo Methods,” Ann. Nucl. Energy 13(2), pp. 63-83 (1986)
4. Denise B. Pelowitz (Ed.), “MCNP6^{TM} User’s Manual – Version 1.0”, Los Alamos National Laboratory, LA-CP-13-00634, Rev. 0 (2013)
5. K.G. Veinot, N.E. Hertel, “Effective quality factors for neutrons based on the revised ICRP/ICRU recommendations,” Radiat. Prot. Dosim. 115 1-4 536 (2005)
6. A. Konobeyev and K. Voukelatou, “Displacement Cross-Sections for Materials Irradiated with Neutrons and Protons at the Energies up to 1 GeV,” ENEA FIS-P894-012 (2005)
7. E.D. Blakeman, “Neutron and Gamma Fluxes and dpa Rates for HFIR Vessel Beltline Region (Present and Upgrade Designs),” ORNL/TM-13693 (2000)

DISTRIBUTION LIST

M. Tarantino	FSN – SICNUC	mariano.tarantino@enea.it
D. Giusti	FSN – PROIN	davide.giusti@enea.it
F. Rocchi	FSN – SICNUC – SIN	federico.rocchi@enea.it
A. Guglielmelli	FSN – SICNUC - SIN	antonio.guglielmelli@enea.it
G. Grasso	FSN – SICNUC - PSSN	giacomo.grasso@enea.it
R. Pergreffi	FSN – SICNUC – PSSN	roberto.pregreffi@enea.it
ARCHIVIO FSN – PROIN		